Nuclear Physics B164 (1980) 445–483


# RADIATIVE CORRECTIONS TO $e^+e^- \to W^+W^-$ IN THE WEINBERG MODEL

M. LEMOINE and M. VELTMAN
*Instituut voor Theoretische Fysica, Princetonplein 5, P.B. 80006, 3508 TA Utrecht, The Netherlands*

Received 6 June 1979

The one-loop radiation corrections to the process $e^+e^- \to W^+W^-$ are calculated in the Weinberg model. The corrections are computed in a c.m. energy range of 180–1000 GeV. The dependence on the Higgs mass is studied in detail; it is found that variations in the Higgs mass from 10–1000 GeV give rise to variations of about 5% in the total cross section.

## 1. Introduction

Recently a new method for the calculation of one-loop radiative corrections has been introduced [1] and applied to $e^+e^- \to \mu^+\mu^-$ [2] and $e^+e^- \to e^+e^-$ [3]. The results of such calculations will be indispensable in the case that electron-positron machines with total energies above 60 GeV become reality.

Yet the most interesting features of weak interaction theory, which we take for definitness to be described by the Weinberg-GIM model [4] are not contained in the above-mentioned processes. To be precise, one may distinguish three different kinds of radiative corrections, namely:

(i) soft photon corrections;
(ii) hard photon and vector boson corrections;
(iii) Higgs-dependent corrections.

The soft photon corrections, while numerically very important, are the least interesting from a physical point of view. These corrections are simply proportional to the lowest-order results and do not probe in any way the deeper structure of the amplitudes. More interesting are hard photon and vector boson type corrections: they are comparable to the Lamb-shift etc., and do depend on the existence of an underlying renormalizable theory.

Certainly most interesting are Higgs-dependent corrections, since they relate to that part of the theory that must be added to obtain a theory finite to all orders. To understand properly the significance of the process considered in this paper it is

perhaps necessary to repeat some of the arguments, that have been given before [5,6].

Without the Higgs sector the Weinberg model reduces to the Glashow model [4], which is non-renormalizable and thus contains infinities for certain observable quantities. This is manifest in the Weinberg model: certain diagrams and amplitudes grow indefinitely if the Higgs mass tends to infinity. One may thus consider the Higgs system as a (physically realizable) cut-off mechanism for the vector boson theory. This, in principle, provides for a method to estimate the Higgs mass even at low energies. One simply measures the radiative corrections to some amplitude that grows relatively fast with rising Higgs mass and then obtains an estimate for this mass.

In order to have a practically realizable method it is necessary to have an amplitude that already becomes infinite at the one-loop level in the limit of large Higgs mass. The reason is that we are dealing with perturbation theory. In the limit of large Higgs mass it turns out that the successive loop approximations amount to a perturbation expansion in terms of the combination $\alpha m^2/M^2$, where $\alpha$ is the fine structure constant, and $m$ and $M$ are the Higgs and vector boson masses respectively. The first divergent term is usually of the form $\alpha \ln(m^2/M^2)$.

Now consider an amplitude that remains finite at the one-loop level. The series expansion will be of the form

$$\alpha + \alpha^2 + \alpha^3 \ln \Lambda + \alpha^4 \Lambda + \alpha^5 \Lambda^2 + \ldots,$$

where $\Lambda = m^2/M^2$. In all reasonableness we cannot expect this amplitude to be very different from the lowest-order results even if $\alpha\Lambda$ is of the order 1 or larger. What we have here can be rewritten in the form

$$\alpha + \alpha^2 + \alpha^3 \ln \Lambda + \alpha^3 R\,,$$

where $R$ is a power series in $\alpha\Lambda$. Naively one would expect $R$ to be of the order 1–10 even if $\alpha\Lambda$ is much larger than one. Of course we have no rational basis for believing this, because perturbation theory is then completely useless, but we say this merely on the basis of our experience in strong interactions.

However, in case the loop-corrections start with $\alpha^2 \ln \Lambda$ or even better with $\alpha^2\Lambda$, then we are in a much more promising situation. Then indeed a precise measurement of the amplitude may give sensible information on the Higgs system.

Analysis of this situation [5] has revealed the following facts.

(i) There is a "screening theorem" which states that for all relevant low-energy processes no observable one-loop radiative corrections of the type $\alpha^2 \ln \Lambda$ (or stronger) exist. To be precise, there is such a correction in the fermion scattering sector, but this correction contains a factor $m_f^2/M^2$, where $m_f$ is the fermion mass, which reduces it to insignificance.

(ii) An exception to this screening theorem can be found in deviations from the symmetry of the theory. More precisely, the radiative corrections to the coupling constant of the three vector boson vertex differ by terms of the form $\alpha \ln \Lambda$ from

comparable corrections to the coupling constant for the vector-boson-fermion vertices *.

This then identifies the only amplitude of interest within the above sketched approach.

In addition there is another aspect that may be mentioned here. Several authors [6] have noted that for large Higgs mass (of the order of 1 TeV) the unitarity limit in elastic vector boson scattering is violated (for longitudinal polarizations). This violation is proportional to the Higgs mass squared and not to the logarithm of this mass. Equivalently, this means that for such a large Higgs mass the higher-order corrections become of the same order of magnitude as the lowest-order corrections. Unfortunately, this strong violation (proportionality to the Higgs mass squared) occurs only in the S-wave part, which in turn is only a small part of the total cross section. In the total cross section very little remains of this effect. Correspondingly the one-loop diagrams are only logarithmically divergent in the limit of large Higgs mass, and the divergence is in the nature of point (ii) above.

Nevertheless in studying the situation in more detail one discovers that there may be surprises in the following sense. All considerations concerning large Higgs masses are based on limiting procedures, where either the Higgs mass, or the c.m. energy is taken to be much larger than anything else. In ref. [5] the Higgs mass is large; in ref. [6] the energy is much larger than anything else including the Higgs mass. Seeming discrepancies between the two approaches may have their origin here. In fact, one is led to the idea that the effects may be particularly enhanced in the region where both the energy and the Higgs mass are of the same order of magnitude but large with respect to the vector boson mass.

All this adds further incentive to the study of the process $e^+e^- \to W^+W^-$. Indeed the WWW vertex occurs in this process, and we therefore expect corrections of the form $\ln \Lambda$. Furthermore, if we are lucky, this logarithm may come out much stronger at large energies as compared to the pessimistic of ref. [5]. There the factor in front of the term $\ln \Lambda$ was found to be of the order of $10^{-4}$.

Clearly nothing short of a complete calculation can clarify the issue. This then is the major goal of this paper. Indeed the term $\ln \Lambda$ is visible and has an effect of order 5% on the cross section. This must not simply be interpreted on its face value; it means in fact that we are sensitive to the series expansion given above.

Evidently the main part of this paper is quite technical, involving the numerical evaluation of many diagrams (of the order of 600). One of the major problems is to ascertain that the results are correct, and this in fact requires much more work than the calculation of the diagrams actually contributing to the cross section. This is because in the end the major tool in this sense is provided by the Ward identities, and these become quite complicated. Incidentally, it is interesting to note that the

* If for the vector boson masses the Higgs $\Delta I = \frac{1}{2}$ rule is assumed, then there is also an $\alpha \ln \Lambda$ correction to this rule.

results involve cancellations of anomalies due to lepton and quark contributions. The prescription of Chanowitz et al. [7] of completely anticommuting $\gamma_5$ has been used in this context. The infrared divergencies are regularized by a small photon mass $\lambda$. In this paper the $\tau$-lepton and associated top and bottom quarks are not considered.

The outline of this paper is as follows. In sect. 2 a summary of the model is presented. The lowest-order cross section is given in sect. 3. Sects. 4–7 deal with the various radiative corrections, and the method used to compute them. Bremsstrahlung and infrared divergencies are discussed in sect. 8, followed by a discussion of the renormalization procedure in sect. 9. The Ward identities are summarized in sect. 10. The leading terms of the amplitude in the limit of large Higgs mass are discussed in sect. 11 and the results are presented in sect. 12. In the appendices some details are given.

## 2. The model

The model used is the Weinberg model enlarged with a quark sector according to the GIM mechanism (ref. [4]). Actually, since the quarks do not play any rôle in this process, except in the cancellation of the anomalies, there is no dependence on the Cabibbo angle. In appendix A of ref. [2] the lagrangian of the model including leptons has been given; in appendix A of this paper the part of the lagrangian containing quarks is written down.

The masses of the charged and neutral vector bosons and the Higgs scalar are denoted by $M$, $M_0$ and $m$. Sin and cos of the weak mixing angle are denoted by $s_\theta$ and $c_\theta$ respectively.

## 3. Lowest order $e^+e^- \to W^+W^-$

In this paper we will use the following notations and conventions (fig. 1). All momenta are incoming and the metric is such that a time-like vector squared is negative. The momenta of the incoming electron and positron and outgoing $W^+W^-$ pair are denoted by $p_1$, $p_2$, $q_1$ and $q_2$, respectively, and $e_1$ and $e_2$ are the polarization

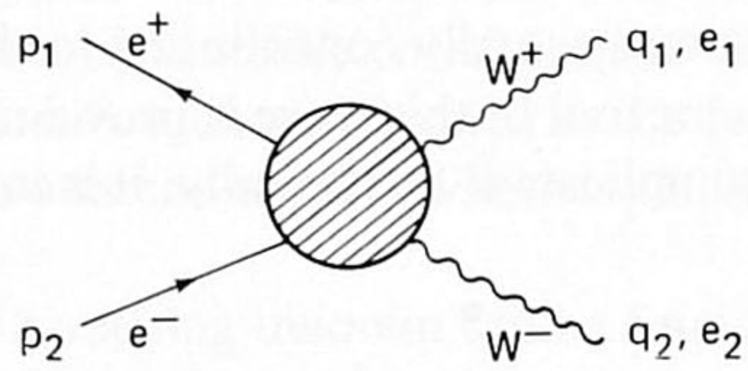


Fig. 1. Amplitude for $e^+e^- \to W^+W^-$.

vectors of $W^+$ and $W^-$. We have:

$$p_1^2 = p_2^2 = -m_e^2 , \qquad q_1^2 = q_2^2 = -M^2 .$$

Furthermore we define

$$S = -(p_1 + p_2)^2 = -(q_1 + q_2)^2 , \qquad s = S/M^2 , \qquad q_{3\mu} = -(q_{1\mu} + q_{2\mu}) ,$$
$$T = -(p_1 + q_1)^2 = -(p_2 + q_2)^2 , \qquad t = T/M^2 , \qquad q_{4\mu} = (q_{2\mu} + p_{2\mu}) .$$

The masses of the charged vector bosons $W^{\pm}$, the neutral vector boson $W^0$ and the physical Higgs-scalar Z are denoted by $M$, $M_0$ and $m$ respectively. For convenience the following functions are used:

$$V_{\mu\nu\lambda}(q_1, q_2, q_3) = \delta_{\mu\lambda}(q_1 - q_3)_\nu + \delta_{\lambda\nu}(q_3 - q_2)_\mu + \delta_{\nu\mu}(q_2 - q_1)_\lambda ,$$
$$P_{\mu\nu\rho\sigma} = 2\delta_{\mu\nu}\delta_{\rho\sigma} - \delta_{\mu\rho}\delta_{\nu\sigma} - \delta_{\mu\sigma}\delta_{\rho\nu} .$$

These two functions are related to the 3- and 4-point vector boson interactions of the Yang-Mills lagrangian.

If $E$ denotes the energy per particle and $\vartheta_{cm}$ the angle between the 3-vectors $\boldsymbol{p}_1$ and $\boldsymbol{q}_1$, then

$$T = m_e^2 + M^2 - 2\sqrt{(E^2 - m_e^2)(E^2 - M^2)}\cos\vartheta_{cm} - 2E^2$$
$$\simeq M^2 - \tfrac{1}{2}S(1 + \beta\cos\vartheta_{cm}) ,$$

with

$$\beta = \sqrt{1 - 4/s} .$$

Throughout this paper we will reserve the symbols $a$ and $b$ with various subscripts for vector and axial vector coefficients of the electron current, $\bar{a}$ and $\bar{b}$ without any subscript are defined as

$$\bar{a} = \frac{4s_\theta^2 - 1}{4c_\theta} , \qquad \bar{b} = \frac{-1}{4c_\theta} .$$

The lowest-order cross section has been calculated before (ref. [8]), and we present here only the most important details. In lowest order we have three diagrams contributing to the amplitude (fig. 2). The contributions to the lowest-order amplitude are:

$$L_\gamma : \quad (2\pi)^4 g^2 s_\theta^2 \frac{\bar{u}(p_1)\gamma_\lambda u(p_2)}{-S} V_{\mu\nu\lambda}(q_1, q_2, q_3) e_{1\mu} e_{2\nu} ,$$

$$L_{W0} : \quad -(2\pi)^4 g^2 c_\theta \frac{\bar{u}(p_1)\gamma_\lambda(\bar{a} + \bar{b}\gamma_5) u(p_2)}{-S + M_0^2} V_{\mu\nu\lambda}(q_1, q_2, q_3) e_{1\mu} e_{2\nu} , \tag{3.2}$$

$$L_\nu : -(2\pi)^4 g^2 \frac{1}{4} \frac{\bar{u}(p_1)\gamma_\mu \not{q}_4 \gamma_\nu(1 + \gamma_5) u(p_2)}{-T} e_{1\mu} e_{2\nu} .$$

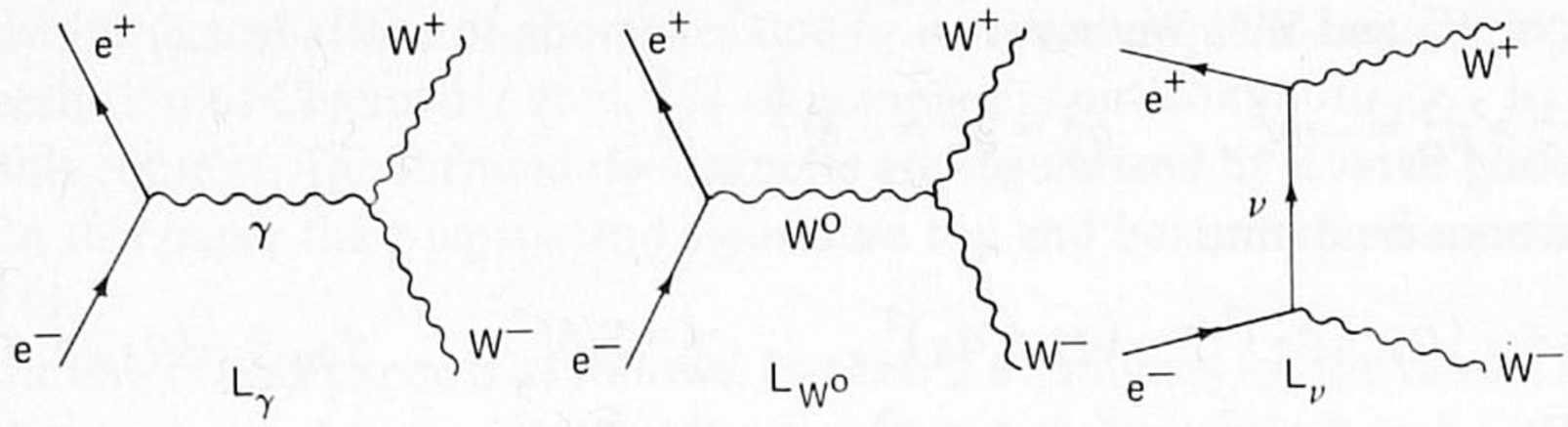


Fig. 2. Lowest-order diagrams.

The corresponding differential cross section is given by

$$d\sigma^0\,[\mathrm{mb}] = g^4\Phi(\sigma^0_{\gamma\gamma} + \sigma^0_{W0W0} + \sigma^0_{\nu\nu} + \sigma^0_{\gamma\nu} + \sigma^0_{W0\nu}) , \tag{3.3}$$

with

$$\Phi = \frac{(0.624)^2\beta}{16(2\pi)^9 S} , \qquad S \text{ expressed in GeV} .$$

The terms inside the brackets correspond to the various terms arising when squaring the amplitude and are given by

$$\sigma^0_{\gamma\gamma} = \frac{s_\theta^4}{S^2} F_1(s,t) , \qquad \sigma^0_{W0W0} = \frac{(\bar{a}^2 + \bar{b}^2)\, c_\theta}{(-S + M_0^2)^2} F_1(s,t) ,$$

$$\sigma^0_{\nu\nu} = \frac{1}{16T^2} F_2(s,t) , \qquad \sigma^0_{\gamma W0} = \frac{-2s_\theta^2 c_\theta (\bar{a} + \bar{b})}{(-S)(-S + M_0^2)} F_1(s,t) , \tag{3.4}$$

$$\sigma^0_{\mu\nu} = \frac{-s_\theta^2}{4ST} F_3(s,t) , \qquad \sigma^0_{W0\nu} = \frac{-c_\theta (\bar{a} + \bar{b})}{4T(-S + M_0^2)} F_3(s,t) .$$

In the case that the final state contains longitudinally polarized vector bosons only, the functions $F_1$, $F_2$ and $F_3$ are given by

$$\left.\begin{aligned} F_1(s,t) &= -2\frac{M^4}{\beta^2}\Delta(s,t)(s+2)^2 , \\ F_2(s,t) &= -4\frac{M^4}{\beta^4}\Delta(s,t)\left(t + \frac{4}{s}\right)^2 , \\ F_3(s,t) &= 4\frac{M^4}{\beta^3}\Delta(s,t)\left(t + \frac{4}{s}\right)(s+2) , \end{aligned}\right\} \text{longitudinal polarization} , \tag{3.5}$$

with

$$\Delta(s,t) = t^2 - 2t + 1 + st .$$

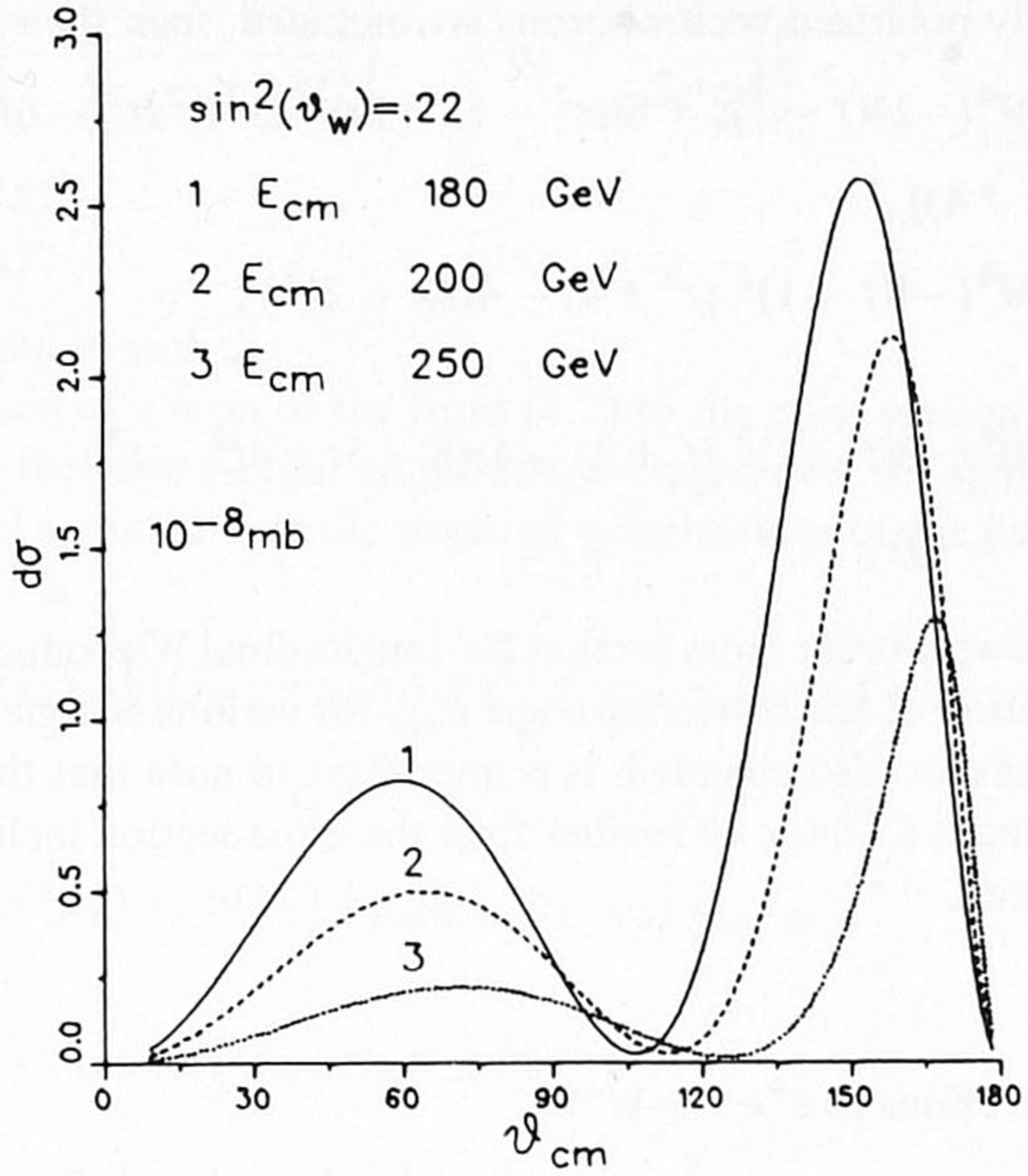


Fig. 3. Differential cross section for longitudinal polarized vector bosons in lowest order.

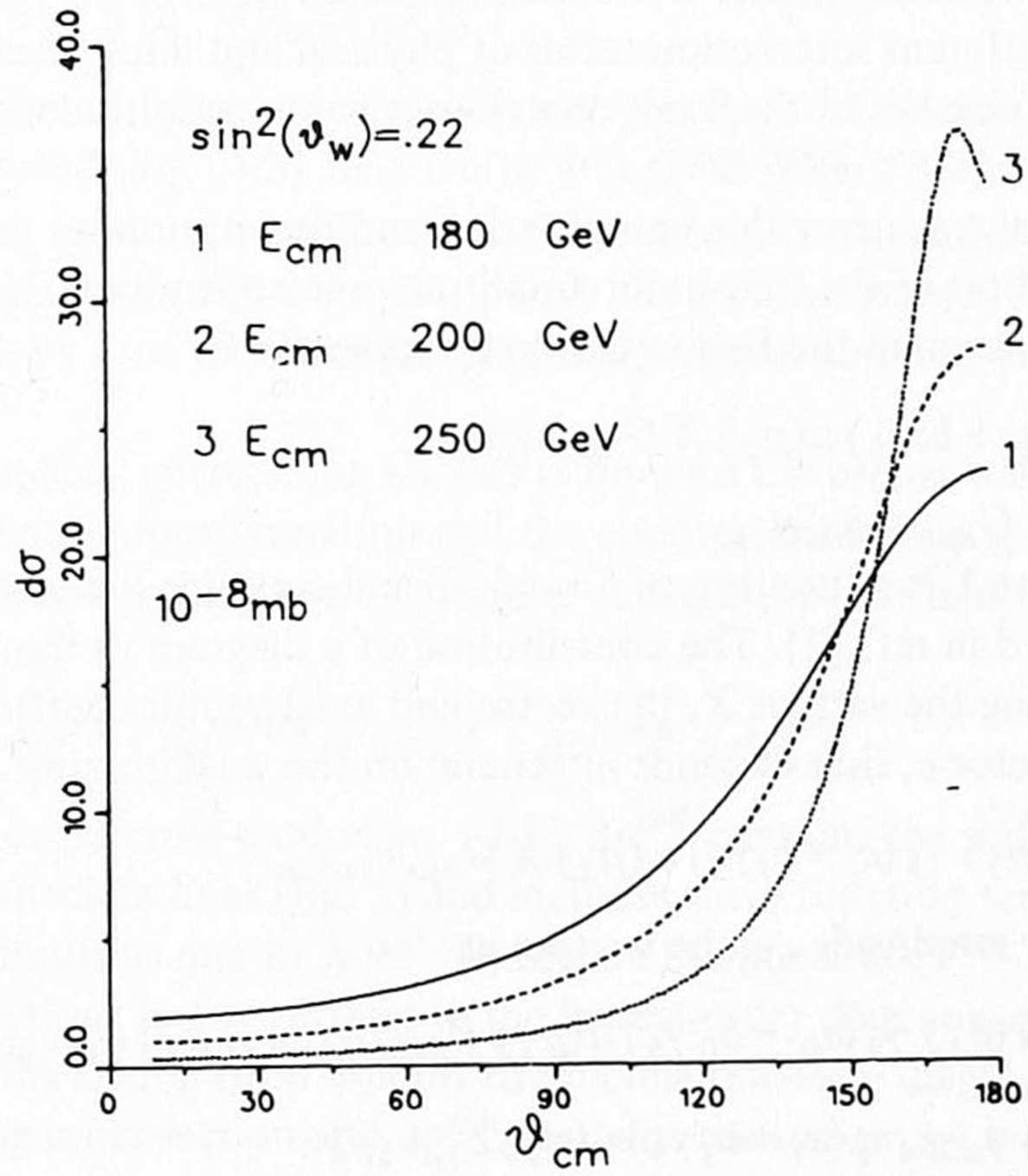


Fig. 4. Differential cross section for $W^+W^-$ production in lowest order.

If the transversally polarized vector bosons are included, then these functions are

$$\left.\begin{aligned} F_1(s,t) &= M^4(-24(t-1)^2 + 8s(t^2-5t+1) - 2s^2(t^2(t^2-6t+17) \\ &\quad - 2s^3(t-4)), \\ F_2(s,t) &= M^4(-4(t-1)^2\,(t^2+4) - 4st(t-2)^2), \\ F_3(s,t) &= M^4(-8(t-1)^2\,(t+2) - 4s(8-5t+4t^2-t^3) \\ &\quad + 4s^2(t^2-4)), \end{aligned}\right\} \text{all polarizations .} \tag{3.6}$$

In fig. 3 the lowest-order cross section for longitudinal W-production has been plotted as a function of the scattering angle $\vartheta_{cm}$ for various energies. In fig. 4 transversal polarizations are also included. It is important to note that the longitudinal cross section is about a factor 10 smaller than the cross section including the transversal vector bosons.

## 4. Radiative corrections to $e^+e^- \to W^+W^-$

Due to the larger symmetry group and the Higgs mechanism the interaction structure of the Weinberg model is more complicated than QED. The lagrangian contains many different interaction terms of physical and unphysical fields and therefore a large number of diagrams contributes to the amplitude and cross section of the process $e^+e^- \to W^+W^-$.

In order to make a surveyable computation and description we define a convenient decomposition of the first-order amplitude, see appendix C. Now consider for example the first term in the first equation of appendix C:

$$\bar{u}(p_1)\,\gamma_\lambda(a_j + b_j\gamma_5)\,u(p_2)\,X\,G_{\lambda\mu\nu}e_{1\mu}e_{2\nu}\,, \tag{4.1}$$

with $X = V_1^b$ and $G_{\lambda\mu\nu} = \delta_{\lambda\nu}q_{1\mu}$.

The coefficient $X$ is a function of $S$ (and $T$) and contains the form factors $A$, $B$, $C$ (and $D$) as defined in ref. [2]. The contribution of a diagram to the amplitude is given by specifying the various $X$, the vector and axial vector coefficients $a_j$ and $b_j$ and an overall factor $c$, that depends in general on the weak mixing angle:

$$g^4 c(s_\theta)\,\bar{u}(p_1)\,\gamma_\lambda(a_j + b_j\gamma_5)\,u(p_2)\,X\,G_{\lambda\mu\nu}e_{1\mu}e_{2\nu}\,. \tag{4.2}$$

The lowest-order amplitude can be written as

$$\begin{aligned} \mathcal{A}_0 = g^2\,\{&\bar{u}(p_1)\,\gamma_\lambda(a_0 + b_0\gamma_5)\,u(p_2)\,V_{\mu\nu\lambda}(q_1,q_2,q_3)\,e_{1\mu}e_{2\nu} \\ &+ \bar{u}(p_1)\,\gamma_\mu\,\not{q}_4\gamma_\nu(a_t + b_t\gamma_5)\,u(p_2)\,e_{1\mu}e_{2\nu}\}\,. \end{aligned} \tag{4.3}$$

The coefficients $a_0$, $b_0$ and $a_t$ and $b_t$ are

$$a_0 = (2\pi)^4 \left\{ -\frac{s_\theta^2}{S} - \frac{\bar{a}\, c_\theta}{-S + M_0^2} \right\}, \qquad b_0 = \frac{(2\pi)^4 \bar{b}\, c_\theta}{-S + M_0^2} \ , \tag{4.4}$$

$$a_t = b_t = \frac{(2\pi)^4}{4T} \ ;$$

$\bar{a}$ and $\bar{b}$ are defined in sect. 2.

The contribution of a term of the form (4.2) to the cross section is given by the interference with the lowest-order amplitude, averaged over the spins of the incoming particles and summed over the required polarizations of the outgoing vector bosons. The result is

$$\sigma_j = 2g^6 \Phi c(s_\theta)\, \mathrm{Re}\left[ (a_0 a_j + b_0 b_j)\, XY^S + (a_t a_j + b_t b_j)\, XY^T \right] , \tag{4.5}$$

with

$$Y^S = \sum_{\text{spin}} \{ \bar{u}(p_1)\, \gamma_\lambda\, u(p_2)\, V_{\mu\nu\lambda}(q_1, q_2, q_3)\, e_{1\mu} e_{2\nu} \}^*$$

$$\times \{ \bar{u}(p_1)\, \gamma_\lambda\, u(p_2)\, G_{\lambda\rho\sigma}\, e_{1\rho} e_{2\sigma} \} ,$$

$$Y^T = \sum_{\text{spin}} \{ \bar{u}(p_1)\, \gamma_\mu \not{q}_4 \gamma_\nu u(p_2)\, e_{1\mu} e_{2\nu} \}^* \tag{4.6}$$

$$\times \{ \bar{u}(p_1)\, \gamma_\lambda\, u(p_2)\, G_{\lambda\rho\sigma} e_{1\rho} e_{2\sigma} \} .$$

$Y^S$ and $Y^T$ correspond to the interference with the $S$- and $T$-channel terms of the lowest-order amplitude eq. (4.3). The factor $\Phi$ is given in eq. (3.3).

In the following sections we will describe the various contributions to the cross section. According to eq. (4.5) we must specify the parameters $c(s_\theta)$, $a_j$ and $b_j$ and the various functions $X$ of the form factors for the vertex and box diagram corrections.

Apart from one-loop corrections we also computed the bremsstrahlung cross section in the soft photon approximation and the counterterms, arising from the renormalization of the weak mixing angle, coupling constant, masses and the wave functions. We write:

$$d\sigma = d\sigma^0 + d\sigma^{\text{self}} + d\sigma^{\text{vertex}} + d\sigma^{\text{box}} + d\sigma^{\text{brem}} + d\sigma^{\text{ren}} \ . \tag{4.7}$$

$d\sigma^0$ is the lowest-order cross section eq. (3.3); $d\sigma^{\text{self}}$ contains the self-energy insertions on the intermediate lines (fig. 2) and includes wave function renormalization terms. Also contributions due to A-$W^0$ mixing are included. $d\sigma^{\text{vertex}}$ is the total contribution of corrections to the vertices in the lowest-order diagrams and $d\sigma^{\text{box}}$ contains the corrections arising from 4-point irreducible one-loop diagrams. $d\sigma^{\text{brem}}$ is the bremsstrahlung cross section and $d\sigma^{\text{ren}}$ contains the remaining renormalization counterterms.

## 5. Self-energy insertions, mixing and wave-function renormalizations

Radiative corrections due to the selfenergy of photon, neutral vector boson and neutrino and due to A-$W^0$ mixing are given by the diagrams of fig. 5.

In spite of the fact that we fixed the gauge in such a way, that vector and scalar fields do not mix at the tree level, mixing arises at the one-loop level. The vector-scalar mixing results in a contribution proportional to the electron mass, and can be neglected. For the amplitude we have to consider A-$W^0$ mixing only. We denote the photon, neutral vector boson, and neutrino self-energy insertions by $\Sigma^{\mathrm{p}}_{\mu\nu}$, $\Sigma^{0}_{\mu\nu}$ and $\Sigma^{\nu}$, respectively. For the mixing we write $\Sigma^{0\mathrm{p}}_{\mu\nu}$. Since the terms proportional to $k_\mu k_\nu$ of $\Sigma^{\mathrm{p}}_{\mu\nu}$, $\Sigma^{0}_{\mu\nu}$ and $\Sigma^{0\mathrm{p}}_{\mu\nu}$ give contributions proportional to the electron mass, only $\delta_{\mu\nu}$ terms in the self-energy insertions and the mixing are of importance. Their coefficients will be denoted by $A^{\mathrm{p}}_1(k^2)$, $A^{0}_1(k^2)$ and $A^{0\mathrm{p}}_1(k^2)$, see appendix B. The self-energy of a neutrino of four-momentum $k$ is proportional to $\not{k}(1+\gamma_5)$:

$$\Sigma^{\nu}(k) = A(k^2)\,\not{k}\tfrac{1}{2}(1+\gamma_5)\,, \tag{5.1}$$

and in terms of form factors one has

$$A^{\nu}(k^2) = B_1(k, m_{\mathrm{e}}, M) + \frac{1}{2c_\theta^2}\,B_1(k, 0, M_0) + \left(\frac{1}{2} + \frac{1}{2c_\theta^2}\right) i\pi^2\,. \tag{5.2}$$

The contribution of the photon self-energy insertion to the cross section is given by

$$-2g^6 s_\theta^2 \Phi\,\frac{\mathrm{Im}[A^{\mathrm{p}}_1(-S)]}{S^2}\;\{a_0 F_1(s, t) + \tfrac{1}{2} a_t F_3(s, t)\}\,, \tag{5.3}$$




Fig. 5. Self-energy insertions and A-$W^0$ mixing.

which is proportional to the imaginary part of $A_1^{\mathrm{p}}(k^2)$, computed at $k^2 = -S$. The quantities $a_0$ and $a_t$ are defined in eq. (4.3a) and the functions $F_i$ in eqs. (3.4), (3.5). $\Phi$ is defined by eq. (3.3).

The contribution due to the self-energy of the neutral vector boson is

$$2g^6 c_\theta \Phi \frac{\mathrm{Im}[A_1^0(-S) - A_1^0(-M_0^2)]}{(-S + M_0^2)^2} \{(\bar{a}\, a_0 + \bar{b} b_0) F_1(s, t) + \tfrac{1}{2}(a_0 + b_0) a_t F_3(s, t)\}, \tag{5.4}$$

with $\bar{a}$ and $\bar{b}$ given in eq. (3.1). In eq. (5.4) we have taken into account the renormalization of the neutral vector boson mass by subtracting $A_1^0(k^2)$, computed at $k^2 = -M_0^2$. We have assumed that the physical mass of the neutral vector boson is given by $M_0$. In sect. 9 we will consider this assumption in more detail. The contribution due to the self-energy of the neutrino is:

$$2g^6 \Phi \frac{\mathrm{Im}[(A^\nu(-T)]}{4T} \{\tfrac{1}{2}(a_0 + b_0) F_3(s, t) + a_t F_2(s, t)\}, \tag{5.5}$$

with $A^\nu$ defined in eq. (5.2). Finally the contributions due to the mixing of photon and neutral vector boson (figs. 5d, e) are, respectively,

$$-2g^6 s_\theta c_\theta \Phi \frac{\mathrm{Im}[A^{0\mathrm{p}}(-S)]}{(-S)(-S + M_0^2)} \{a_0 F_1(s, t) + \tfrac{1}{2} a_t F_3(s, t)\}, \tag{5.6}$$

$$2g^6 s_\theta \Phi \frac{\mathrm{Im}[A^{0\mathrm{p}}(-S)]}{(-S)(-S + M_0^2)} \{(a_0 \bar{a} + b_0 \bar{b}) F_1(s, t) + \tfrac{1}{2}(\bar{a} + \bar{b}) a_t F_3(s, t)\}. \tag{5.7}$$

Next we compute the electron and charged vector boson wave-function renormalizations. These renormalization factors can be calculated by considering the residue at the pole of the one-loop corrected propagators.

For the renormalization of the electron and positron wave functions we need the self-energy contributions corresponding to the diagrams of fig. 6. One finds

$$\begin{aligned} S_1 &= i\not{p}\, s_\theta^2 (2B_1(p, m_\mathrm{e}, \lambda) + i\pi^2) + m_\mathrm{e}(-4s_\theta^2 B_0(p, m_\mathrm{e}, \lambda) + 2s_\theta^2\, i\pi^2), \\ S_2 &= i\not{p}\, \{(\bar{a}^2 + \bar{b}^2 + 2\bar{a}\,\bar{b}\,\gamma_5)(2B_1(p, m_\mathrm{e}, M_0) + i\pi^2)\} \\ &\quad + m_\mathrm{e}(\bar{a}^2 + \bar{b}^2)(-4B_0(p, m_\mathrm{e}, M_0) + 2i\pi^2), \\ S_3 &= i\not{p}\,(1 + \gamma_5)(\tfrac{1}{2}B_1(p, 0, M) + \tfrac{1}{4}\, i\pi^2). \end{aligned} \tag{5.8}$$

The one-loop dressed propagator of the electron is

$$D(p) = [(2\pi)^4\, i]^{-1} \{i\not{p} + m_\mathrm{e} - \Sigma(p)/(2\pi)^4 i\}^{-1},$$

with $\Sigma(p) = S_1 + S_2 + S_3$. Let us write the self-energy of the electron as

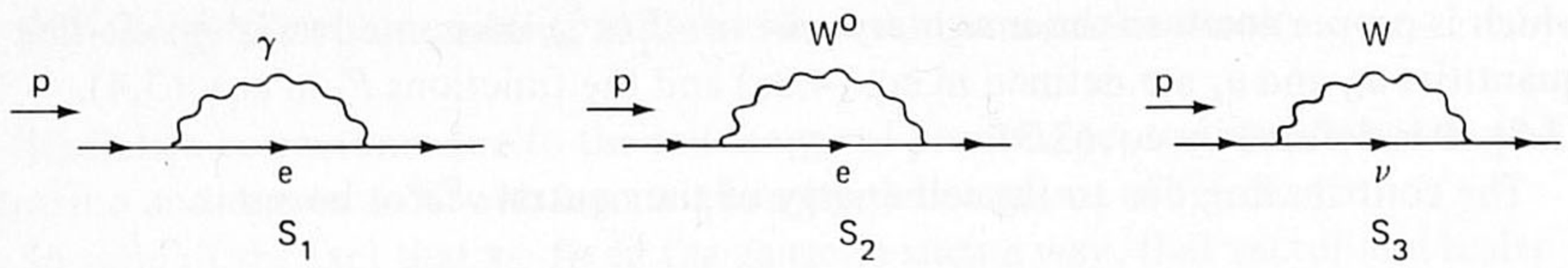


Fig. 6. Self-energy insertions for the electron.

$$\Sigma(p) = (2\pi)^4 i\,[i\not{p}(A + B\gamma_5) + m_e C]\ . \tag{5.9}$$

Then the dressed propagator is

$$D(p) = \frac{1}{(2\pi)^4 i}\,\frac{-i\not{p}\,(1 - A - B\gamma_5) + m_e(1 - C)}{p^2(1 - 2A) + m_e^2(1 - 2C)}\ . \tag{5.10}$$

Requiring a pole at $p^2 = -m_e^2$, the renormalization of the electron mass is

$$\delta m_e^2 = 2m_e^2(\underline{C} - \underline{A})\,.$$

$\underline{C}$ and $\underline{A}$ are the functions $C$ and $A$ computed at the pole $p^2 = -m_e^2$. Expanding the dressed propagator equation (5.10) in $(p^2 + m_e^2)$, we have

$$D(p) = \frac{1}{(2\pi)^4 i\,(p^2 + m_e^2)}\{-i\not{p}\,(1 + \underline{A} - 2m_e^2(A' - \underline{C}') - B\gamma_5)$$
$$+ m_e(1 + \underline{A} - 2m_e^2(\underline{A}' - C')) + \mathrm{O}(p^2 + m_e^2\}\ . \tag{5.11}$$

Therefore the renormalized wave functions are

incoming electron: $(1 + Z_1 + Z_2\gamma_5)\,u(p_2)$,

outgoing positron: $-\bar{u}\,(p_1)\,(1 + Z_1 - Z_2\gamma_5)$,

with

$$Z_1 = \tfrac{1}{2}g^2(\underline{A} - 2m_e^2(\underline{A}' - C'))\,,$$
$$Z_2 = \tfrac{1}{2}g^2 B\ . \tag{5.12}$$

The functions $A$, $B$ and $C$ are to be determined by writing eq. (5.8) in the form (5.9). Further $\underline{A}$, $\underline{B}$ and $\underline{C}$ are the values of these functions at the pole $p^2 = -m_e^2$, and $\underline{C}'$ and $A'$ are derivatives of the functions $C$ and $A$ with respect to $p^2$, computed at $p^2 = -m_e^2$. Since the contribution to $(\underline{A}' - C')$ of diagram $S_1$ is infrared divergent and of the form

$$\frac{1}{m_e^2}\ln\frac{\lambda^2}{m_e^2}\,,$$

we cannot neglect the term $2m_e^2(\underline{A}' - \underline{C}')$ in $Z_1$. Note that the left-handed and right-handed electron have different wave-function renormalizations. The terms in the cross

section due to the electron wave-function renormalization are

in the photon channel ($L_\gamma$):

$$\frac{4g^4(2\pi)^4 s_\theta^2 \Phi}{S} \{(Z_1 a_0 + Z_2 b_0) F_1(s, t) + \tfrac{1}{2}(Z_1 + Z_2) a_t F_3(s, t)\}; \qquad (5.13)$$

in the neutral vector boson-channel ($L_{W0}$):

$$\frac{4g^4(2\pi)^4 c_\theta \Phi}{-S + M_0^2} \{((\bar{a} Z_1 + \bar{b} Z_2) a_0 + (\bar{a} Z_2 + \bar{b} Z_1) b_0) F_1(s, t)$$

$$+ \tfrac{1}{2}(Z_1 + Z_2)(\bar{a} + \bar{b}) a_t F_3(s, t)\}; \qquad (5.14)$$

and in the neutrino-channel ($L_\nu$):

$$\frac{4g^4(2\pi)^4 (Z_1 + Z_2) \Phi}{4T} \{\tfrac{1}{2}(a_0 + b_0) F_3(s, t) + a_t F_2(s, t)\}. \qquad (5.15)$$

The infrared divergences factorize in the usual way.

The wave-function renormalization for the charged vector boson is determined by the self-energy $\Sigma^c_{\mu\nu}$, more precisely the term $A_1^c(k^2)\,\delta_{\mu\nu}$. In appendix B, $\Sigma^c_{\mu\nu}$ is expressed in terms of form factors. The renormalized wave function of the charged vector bosons is correspondingly given by:

$$\left\{1 + \frac{1}{2}\frac{g^2}{(2\pi)^4} \operatorname{Im}\left(\frac{\mathrm{d}}{\mathrm{d}k^2} A_1^c(k^2)\Big|_{k^2=-M^2}\right)\right\} e_{i\mu},$$

and the contribution to the cross section is

$$\frac{g^2}{(2\pi)^4} \operatorname{Im}\left(\frac{\mathrm{d}}{\mathrm{d}k^2} A_1^c(k^2)\Big|_{k^2=-M^2}\right) \mathrm{d}\sigma^0, \qquad (5.16)$$

with $\mathrm{d}\sigma^0$ the lowest-order cross section equation, (3.3). The infrared divergence of the wave-function renormalization is due to the diagrams of fig. 7. According to appendix B the infrared-divergent part is

$$i\pi^2 \ln \frac{\lambda^2}{M^2}.$$

Again the infrared divergence factorizes.

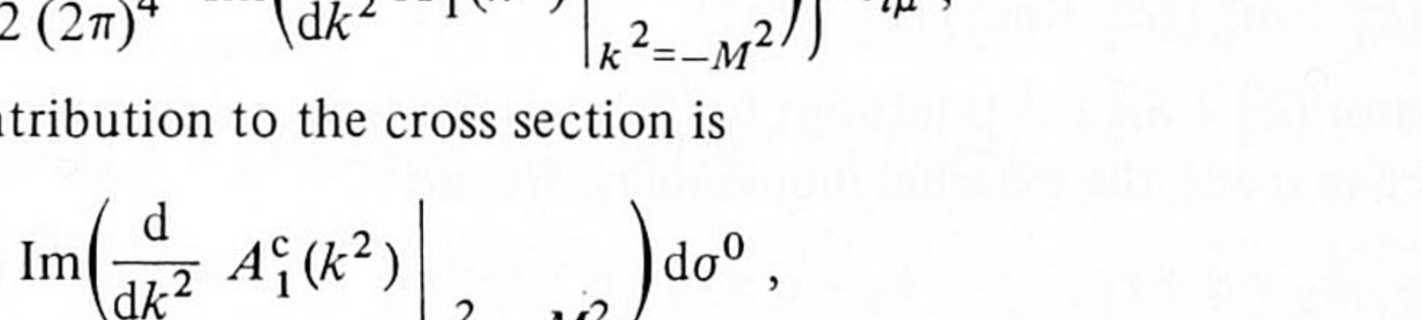


Fig. 7. Infrared-divergent self-energy diagrams for $W^+$, $W^-$ vector bosons.

## 6. Vertex corrections

In this section we describe the contribution to the cross section due to the one-loop corrections to the vertices of the lowest-order diagrams (fig. 2). As stated before, every one-loop correction can be written in the form (4.1), or more explicitly as $\mathcal{A}_1$ (appendix C) and to every such correction certain factors $X_i$ correspond, or more specifically for the contributions due to vertex corrections the factors $V_i^{\mathrm{b}}$, $V_{1i}^{\mathrm{f}}$, $V_{2i}^{\mathrm{f}}$ of appendix C. In other words, every vertex correction must be written in the form $\mathcal{A}_1$, and this determines the $V_i^{\mathrm{b}}$ etc., in terms of the form factors $A$, $B$ and $C$. Finally these $V_i^{\mathrm{b}}$ must be substituted for $X$ in eq. (4.5) together with the corresponding $Y_i^S$ and $Y_i^T$, to set the contribution to the cross section. Of course, also the coefficients $a_j$ and $b_j$, as well as the overall factor $c(s_\theta)$ must be specified.

Analogously to the case of the self-energy diagrams (appendix B) we use certain generic expressions for vertex diagrams. First we distinguish two different topologies for the vertex diagrams of fig. 8. The $r_i$ denote the momenta and the $L_i$ the Lorentz or spinor indices of the external lines. Further $k_i$ and $m_i$ correspond to the momenta and masses of the internal lines.

In the case of the topology-T2, diagrams that have the external lines connected in the same order, are taken together.

In the notation shown in fig. 8 a vertex-correction with the T1 topology, except for an overall factor, can be written as:

$$\int \mathrm{d}q \, \frac{N(k_i, r_i, L_i)}{(k_1^2 + m_1^2)\,(k_2^2 + m_2^2)\,(k_3^2 + m_3^2)} \,. \tag{6.1}$$

The propagator $(k_3^2 + m_3^2)^{-1}$ is left out for T2. $q$ is the loop momentum and the $k_i$ are expressed in $q$ and the external momenta $r_i$. We use

$$k_1 = q\,,\; k_2 = q + r_1\,, \qquad k_3 = q + r_1 + r_2\,, \tag{6.1a}$$

for T1, and

$$k_1 = q\,, \qquad k_2 = q + r_3 \tag{6.1b}$$

for the topology T2.

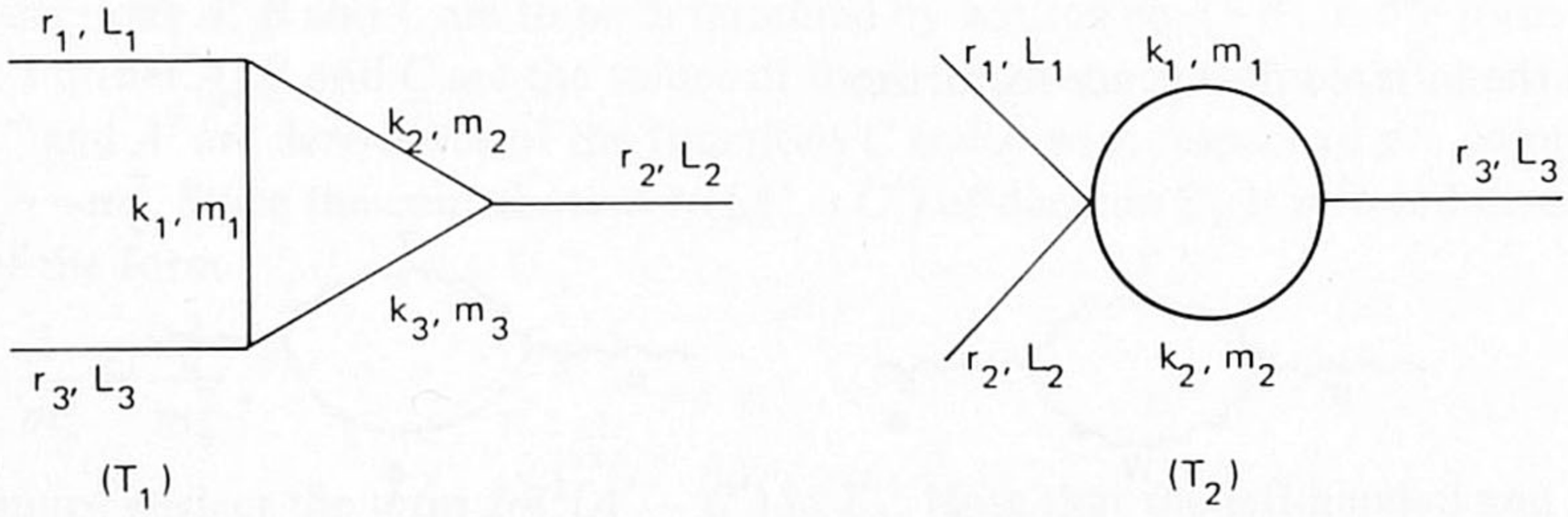


Fig. 8. Topologies of vertex corrections.

The numerator $N$ of (6.1) is in general a function of the internal and external momenta and of the indices $L_i$. The set of generic expressions for the vertex corrections is defined by the numerators of 6.1) and these numerators specify uniquely the form factor functions $X_i$. Therefore the contribution of a vertex-correction to the amplitude is completely determined once the generic numerators and the coefficients $c$, $a_j$ and $b_j$ are given.

Due to the large amount of space required it is actually unfeasible to present all the generic numerators and other details of the various corrections to $e^+e^-A$, $e^+e^-W^0$, $e^+\nu W$, $AW^+W^-$ and $W^0W^+W^-$ vertices. However, the method used will be illustrated by the following example.

*Example*

Consider the vertex correction to the $W^0W^+W^-$ vertex shown in fig. 9. For this vertex correction the following generic numerator in the loop-integral (6.1) was used:

$$N(k_i, r_i, L_i) = -V_{L_2L_1L_3}(k_3, -k_1, r_3)$$
$$= -\{\delta_{L_2L_3}(k_3 - r_3)_{L_1} + \delta_{L_3L_1}(r_3 + k_1)_{L_2} + \delta_{L_1L_2}(-k_1 - k_3)_{L_3}\}.$$

The pairs $(r_1, L_1)$, $(r_2, L_2)$ and $(r_3, L_3)$ correspond in this case to $(q_1, \mu)$, $(q_2, \nu)$ and $(q_3, \lambda)$. Substituting these momenta and indices and the $k_i$ according to eq. (6.1a), the loop-integral can be expressed in the form factors $C$ of ref. [2]. Conforming to the notation of appendix $C$ we find for the expression (6.1) in this case the result:

$$V_1^b \delta_{\lambda\nu} q_{1\mu} + V_2^b \delta_{\lambda\nu} q_{2\mu} + V_3^b \delta_{\lambda\mu} q_{1\nu} + V_4^b \delta_{\lambda\mu} q_{2\nu}$$
$$+ V_5^b \delta_{\mu\nu} q_{1\lambda} + V_6^b \delta_{\mu\nu} q_{2\lambda}, \qquad (6.2)$$

with

$$V_1^b = \mathrm{Im}(-C_{11} - 2C_0), \qquad V_2^b = \mathrm{Im}(-C_{12} - 2C_0),$$
$$V_3^b = \mathrm{Im}(-C_{11} + C_0), \qquad V_4^b = \mathrm{Im}(-C_{12} + C_0),$$
$$V_5^b = \mathrm{Im}(2C_{11} + C_0), \qquad V_6^b = \mathrm{Im}(2C_{12} + C_0).$$

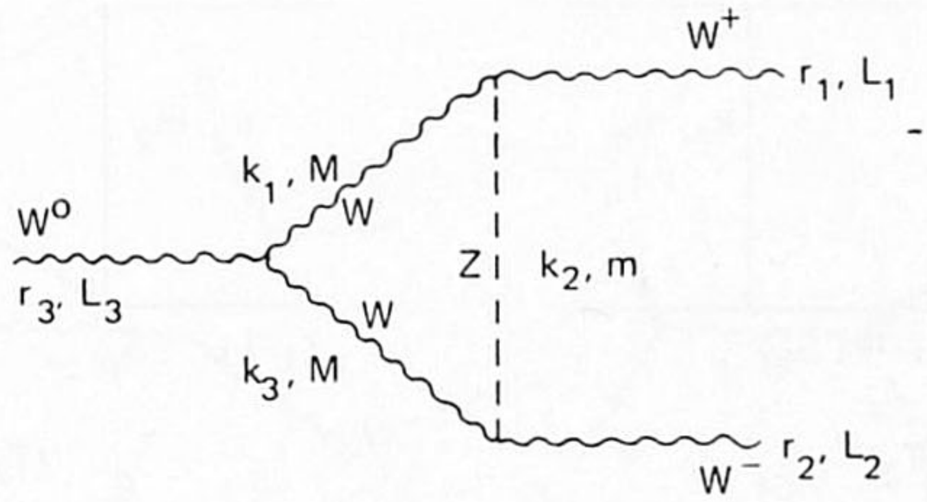


Fig. 9. A $W^0W^+W^-$ vertex correction.

The form factors $C$ are calculated with the internal masses $m_1, m_2, m_3 = M, m, M$, Finally from the Feynman rules we derive an overall factor

$$c(s_\theta) = c_\theta M^2 \ .$$

In order to give the contribution to the amplitude we must multiply (6.2) by

$$\bar{u}(p_1)\,\gamma_\lambda(a_j + b_j\gamma_5)\,u(p_2)\,e_{1\mu}e_{2\nu} \ ,$$

with

$$a_j = \frac{-\bar{a}}{-S + M_0^2} \ , \qquad b_j = \frac{-\bar{b}}{-S + M_0^2} \ .$$

This result is of the form $\mathcal{A}_1$ and the contribution to the cross section follows from (4.5). This concludes the treatment of this particular diagram.

We want now to focus on two details of the vertex-corrections.

(i) The one-loop correction to the $e^+e^-A$ vertex actually contains an ultraviolet-divergent $\gamma_\mu\gamma_5$ piece. In the end these contributions cancel out. This is also required by the theory. If there was no complete cancellation of these divergences that a separate renormalization of the U(1) coupling constants $g_2$ and $g_3$ for the left-handed and right-handed electron, respectively, would have been necessary. However, this is not possible since the relation $g_1 = g_2 + g_3$ (where $g_1$ is the U(1) coupling constant of the Higgs system) must hold. This is because the interaction terms between electron and Higgs scalars generating the mass of the electron must be gauge invariant. Note that $g_1$ in fact determines the mass ratio of the neutral and charged vector bosons, while $g_2$ and $g_3$ determine the weak mixing angle as occurring in the vector-boson-electron interaction. In other words in the Weinberg model, with its simple Higgs structure, there is only one weak mixing angle that can be renormalized.

(ii) Due to the addition of the quark fields to the Weinberg model, the corrections to the $AW^+W^-$ and $W^0W^+W^-$ vertices are free of anomalies. As shown in ref. [7], this can be most easily implemented by the rule that $\gamma_5$ anticommutes with all other $\gamma$ matrices.

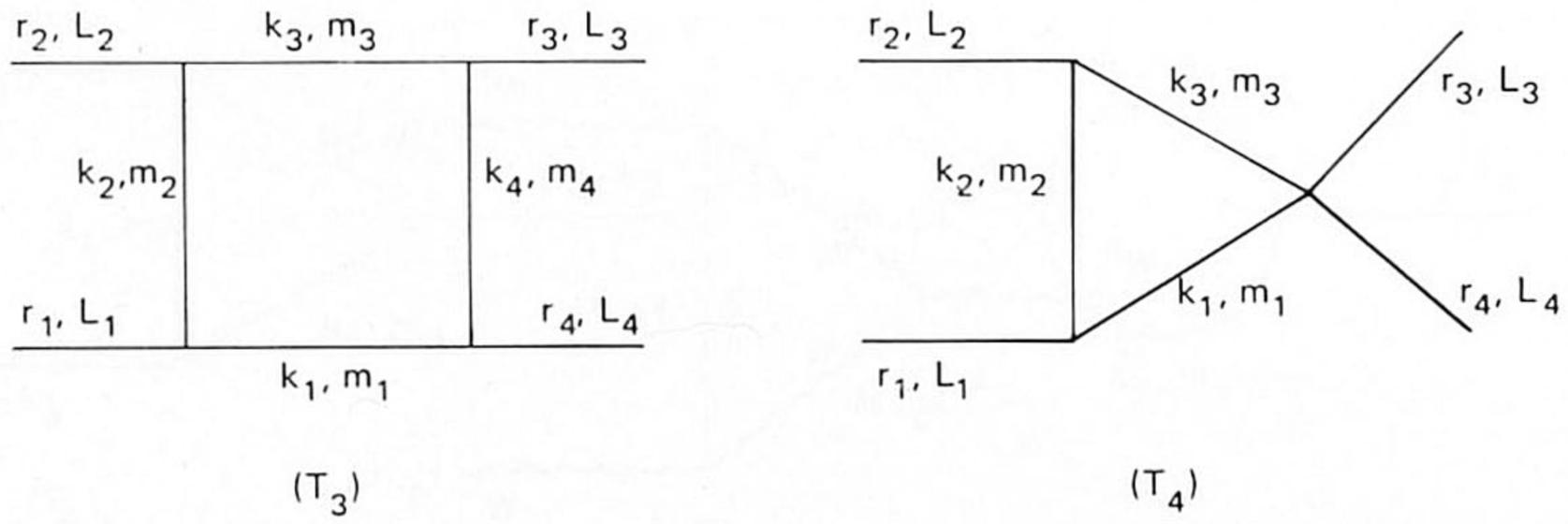


Fig. 10. Topologies of 4-point irreducible one-loop diagrams.

## 7. Box diagram corrections

Analogously to the case of the vertex corrections a certain set of generic box diagrams is defined and the various corrections are classified according to this set. Using a similar notation as in fig. 8 we distinguish two different topologies for the 4-point one-loop irreducible diagram (fig. 10). For the topology T3 the loop-integral (6.1) is defined with the additional propagator $(k_4^2 + m_4^2)^{-1}$. The expressions for the generic diagrams can again be written in the form $\mathcal{A}_S$ with the functions $X_i$, in this case the $B_i^x$, expressed in terms of the formfactors $A$, $B$, $C$ and $D$.

## 8. Bremsstrahlung cross section and infrared-divergent one-loop corrections

The vanishing photon mass causes infrared divergences of the radiative corrections discussed above. In the computation these divergences are regularized by a small photon mass $\lambda$. This causes breaking of the e.m. gauge invariance of the theory, and in fact Ward identities hold apart from terms proportional to $\lambda$. However the divergencies are at worst as $\ln \lambda$, and thus in the limit $\lambda \to 0$ the symmetry is restored.

As in QED we computed the bremsstrahlung cross section $e^+e^- \to W^+W^-\gamma$ in the soft photon limit. The amplitude of this process is given by the diagrams of fig. 11.

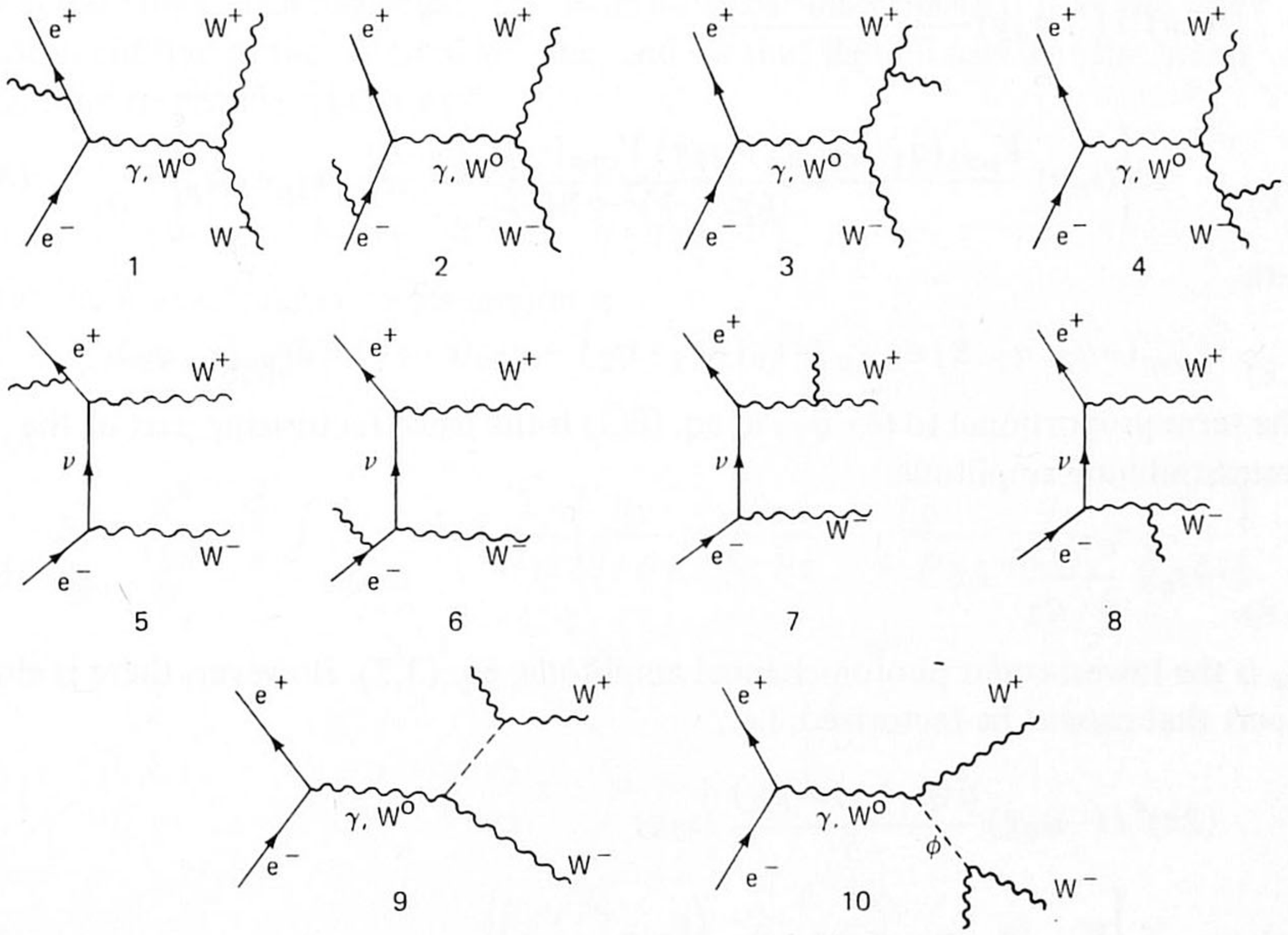


Fig. 11. Diagrams of Bremsstrahlung amplitude.

Let us denote the momentum and polarization vector of the soft photon by $k$ and $e$. In the soft photon limit, the expressions for the diagrams which have the photon emitted from an external fermion line, factorize into some coefficient and the corresponding lowest-order amplitude $L_\gamma$, $L_{W0}$ and $L_\nu$ (fig. 2). For instance the expression for diagram 1 with an intermediate photon is given by

$$-igs_\theta \bar{u}(p_1)\not{e}\ \frac{\{i(\not{p}_1 - \not{k}) + m_e\}}{(p_1 - k)^2 + m_e^2}\left\{\frac{(2\pi)^4 g^2 s_\theta^2}{-S}\ \gamma_\lambda u(p_2)\, V_{\mu\rho\nu\lambda}(q_1, q_2, q_3)\right\} e_{1\mu} e_{2\nu}\,,$$

and is in the soft photon limit equal to

$$-gs_\theta\left(\frac{e\cdot p_1}{k\cdot p_1}\right)\left((2\pi)^4 g^2 s_\theta^2\,\frac{\bar{u}(p_1)\,\gamma_\lambda\, u(p_2)}{-S}\ V_{\mu\nu\lambda}(q_1, q_2, q_3)\, e_{1\mu} e_{2\nu}\right). \quad (8.1)$$

The part in the soft bremsstrahlung amplitude, which corresponds to the diagrams 1, 2, 5 and 6 is

$$-gs_\theta\left(\frac{e\cdot p_1}{k\cdot p_1} - \frac{e\cdot p_2}{k\cdot p_2}\right)\mathcal{A}_0\,. \quad (8.2)$$

The factorization for the expressions of the diagrams, which have the photon emitted from the external vector boson lines, is not obvious, due to our choice of gauge.

Consider diagram 4 with an intermediate photon. The expression corresponding to this diagram is in the soft photon limit

$$(2\pi)^4 i\,(-is_\theta g)\,\frac{\bar{u}(p_1)\,\gamma_\lambda u(p_2)}{-S}$$

$$\times\left\{(s_\theta g)\,\frac{V_{\mu\sigma\lambda}(q_1, q_2, q_3)\,(s_\theta g)\,V_{\sigma\nu\rho}(-q_2, q_2, k)}{((q_2 - k)^2 + M^2)}\ e_{1\mu} e_{2\nu} e_\rho\right\} \quad (8.3)$$

with

$$V_{\sigma\nu\rho}(-q_2, q_2, k)\, e_{2\nu} e_\rho \approx e_\sigma(-e_2\cdot q_2) - q_{2\sigma}(e\cdot e_2) + 2e_{2\sigma}(e\cdot q_2).$$

The term proportional to $(e\cdot q_2)$ in eq. (8.3) is the usual factorizing part of the bremsstrahlung amplitude:

$$-s_\theta g\,\frac{e\cdot q_2}{k\cdot q_2}\ L_\gamma\,. \quad (8.4)$$

$L_\gamma$ is the lowest-order photon-channel amplitude, eq. (3.2). However, there is also a part that cannot be factorized, i.e.,

$$(2\pi)^4 i\,(-is_\theta g)\,\frac{\bar{u}(p_1)\,\gamma_\lambda u(p_2)}{-S}\ (s_\theta g)$$

$$\times\left\{V_{\mu\nu\lambda}(q_1, q_2, q_3)\, e_{1\mu} q_{2\nu}\left(\tfrac{1}{2} s_\theta g\,\frac{e\cdot e_2}{k\cdot q_2}\right)\right\}. \quad (8.5)$$

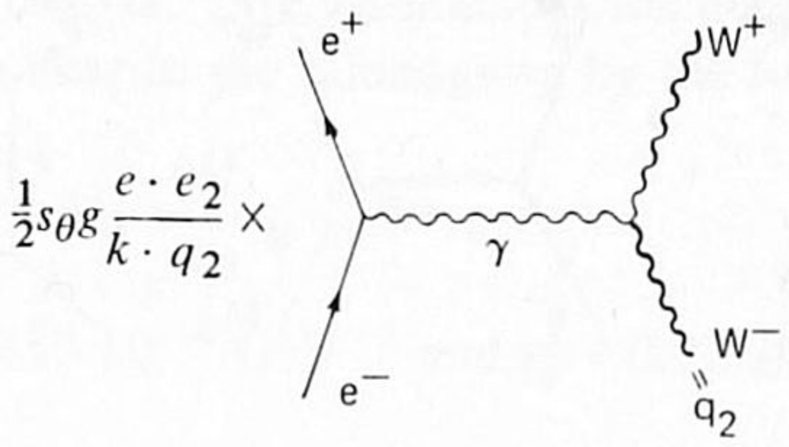


Fig. 12.

Apparently, the polarization vector $e_2$ is replaced by the momentum $q_2$ in the amplitude $L_\gamma$. Diagrammatically this term can be presented as shown in fig. 12. Similar non-factorizing and factorizing terms arise in the neutral vector boson channel and neutrino channel.

Consider now diagram 10 of fig. 11 with an intermediate photon. In the soft photon limit the corresponding expression is

$$(2\pi)^4 i\,(-igs_\theta)\,\frac{\bar{u}(p_1)\,\gamma_\lambda\,u(p_2)}{-S}\,(igs_\theta M)^2\left(e_{1\lambda}\,\frac{e\cdot e_2}{2k\cdot q_2}\right), \tag{8.6}$$

which corresponds to the fig. 13. At the external $\phi$-line we have indicated a factor $M$. We now see that the non-factorizing part of the bremsstrahlung amplitude, which has the photon emitted at the external $W^-$ line, vanishes due to a Ward identity for the lowest order amplitude (fig. 14). Couplings of the $\phi$-fields to the $\nu$-e system have been neglected. The same holds for diagrams that have the soft photon emitted at the external $W^+$ line, and we find that all together the bremsstrahlung amplitude factorizes:

$$-gs_\theta\left\{\frac{e\cdot p_1}{k\cdot p_1}-\frac{e\cdot p_2}{k\cdot p_2}-\frac{e\cdot q_1}{k\cdot q_1}+\frac{e\cdot q_2}{k\cdot q_2}\right\}\mathcal{A}_0\,. \tag{8.7}$$

Thus the bremsstrahlung cross section is

$$\mathrm{d}\sigma^{\mathrm{brem}} = B_{\mathrm{r}}\,\mathrm{d}\sigma^0 \tag{8.8}$$

with

$$B_{\mathrm{r}} = \frac{g^2}{16\pi^2}\,\frac{s_\theta^2}{\pi}\int_{|\boldsymbol{k}|<\omega}\mathrm{d}_3\boldsymbol{k}\,\frac{1}{|k_0|}\left\{\frac{p_1}{k\cdot p_1}-\frac{p_2}{k\cdot p_2}-\frac{p_2}{k\cdot p_2}-\frac{q_1}{k\cdot q_1}+\frac{q_2}{k\cdot q_2}\right\}^2, \tag{8.9}$$

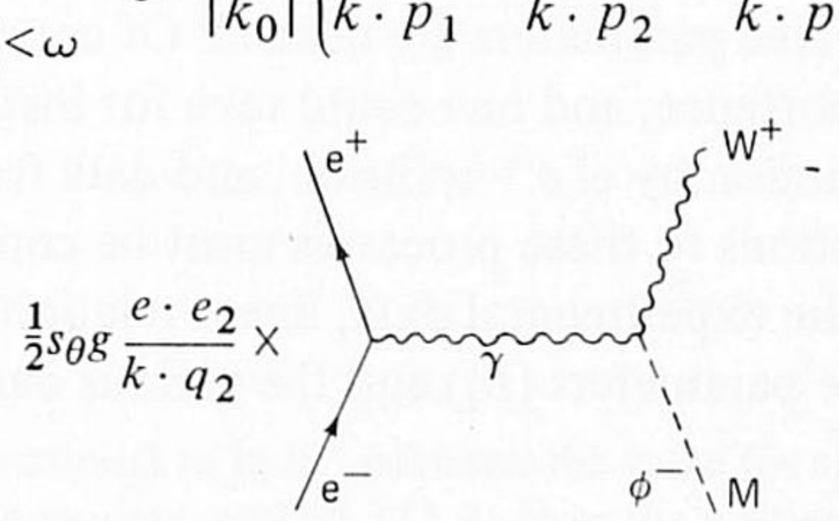


Fig. 13.

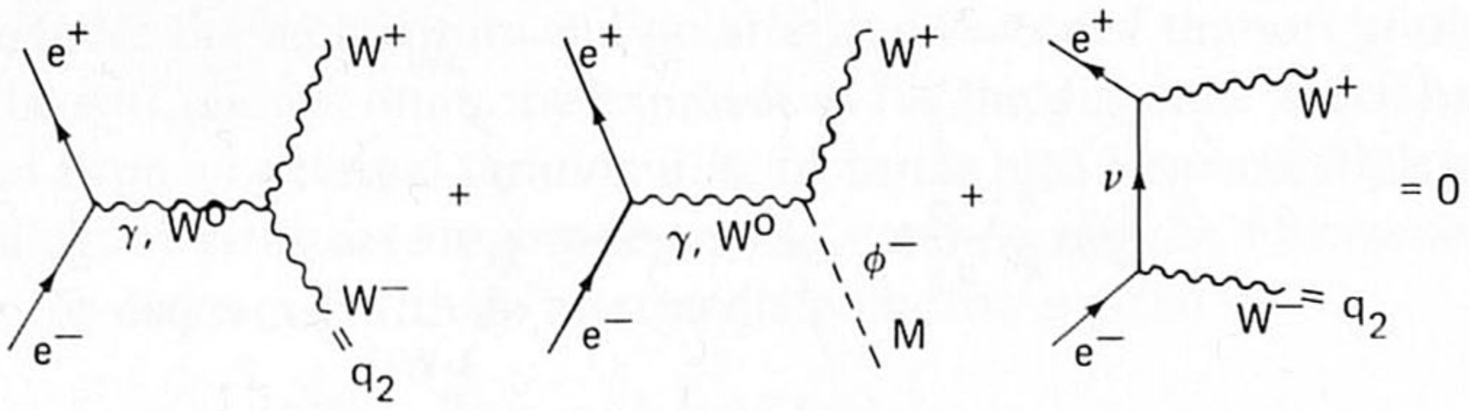


Fig. 14. Ward identity for the lowest-order amplitude.

and $k^2 = -\lambda^2$.

In order to fix the upper limit of the integration $\omega$, the phase space of the photon must be considered (refs. [9–11]).

$$\omega = -\tfrac{1}{2}\left\{E_{\text{th}} - \sqrt{S} + \sqrt{E_{\text{th}}^2 + M^2} - \frac{M^2}{E_{\text{th}} - \sqrt{S} - \sqrt{E_{\text{th}}^2 - M^2}}\right\}. \tag{8.10}$$

$E_{\text{th}}$ is the threshold energy at which the vector bosons can be detected. In the calculation we used that $E_{\text{th}} = 0.45\sqrt{S} = 0.9\, E_{\text{beam}}$.

If the soft bremsstrahlung is added to the other radiative corrections, it is expected that the ln $\lambda$ dependence cancels out. This indeed turns out to be the case, as we have verified numerically. In fact the total tends to a constant as $\lambda$ goes to zero.

## 9. Renormalization

In general the one-loop corrections to the amplitude are ultraviolet divergent and in the dimensional regularization scheme these divergences appear as poles in $(n-4)$, with $n$ the dimension of space-time. These terms must be renormalized away by adding counterterms to the lagrangian, and by taking into account these additional terms in the amplitude. At the end, the free parameters, in this case the coupling constant $g$, the weak mixing angle, and the mass of the charged vector boson $M$, must be fixed by data from experiments, described by the same theory. As many data points as free parameters are needed. Of course the choice of these data points is of no importance, and one could take for instance the leftime of the muon, muon pair production by $e^+e^-$ collision, and data from neutrino experiments. Radiative corrections to these processes must be computed too, and comparing these results with the experimental data, linear relations for the finite renormalization ($\delta p_i$) of the free parameters ($p_i$) and the various data ($d_i$) can be derived:

$$\delta p_i = M_{ij} d_j \,. \tag{9.1}$$

However, we will avoid part of these calculations and make an assumption for

the masses of the vector bosons ★. We assume that the masses of the charged and neutral vector bosons are near to the values given by the following formulae:

$$M^2 = \frac{1}{2}\frac{\alpha\pi}{G_F s_\theta^2}, \qquad M_0 = \frac{M}{c_\theta}, \tag{9.2}$$

where $\alpha = \frac{1}{137}$, $G_F = 8.245 \cdot 10^{-6}$ GeV$^{-2}$ and $s_\theta^2 = 0.22$. This gives $M = 79.5$ GeV and $M_0 = 90.0$ GeV.

As a consequence of this procedure the mass renormalization of the vector bosons is completely determined by the self-energies. The result is (see sect. 5):

$$\text{for charged vector boson:} \qquad \delta M^2 = A_1^c(k^2)|_{k^2=-M^2},$$

$$\text{for neutral vector boson:} \qquad \delta M_0^2 = A_1^0(k^2)|_{k^2=-M_0^2}. \tag{9.3}$$

Since the ratio of the bare charged and neutral vector boson mass is the cos of the bare weak mixing angle, the renormalization of that angle is completely determined by

$$\frac{M^2 + \delta M^2}{M_0^2 + \delta M_0^2} = c_\theta^2 + \delta c_\theta^2, \tag{9.4}$$

or

$$\delta s_\theta^2 = -\frac{\delta M^2 - c_\theta^2 \delta M_0^2}{M_0^2}.$$

Finally we must consider the coupling constant $g$. For the process $e^+e^- \to W^+W^-$ no experimental data are available. However, recently the radiative corrections to $e^+e^- \to \mu^+\mu^-$ were computed (ref. [2]). In this computation the same procedure was followed for the renormalization of the vector boson masses. There the coupling constant was fixed by means of a data point at low energy, and we can simply use the results of that calculation in order to fix $g$. Some extensions were needed since no quark contributions to the self-energies and mixing were taken into account in that paper.

In ref. [2] $\alpha$ was used as a free parameter, because the renormalization was based on the requirement that in the lower energy region ($\sqrt{s} = 0.275$ GeV) the cross section reproduces QED

Since

$$\alpha = \frac{e^2}{4\pi} = \frac{g^2 s_\theta^2}{4\pi},$$

it follows that

★ There is a difference proportional to $\ln m^2$ between the value for $s_\theta^2$ determined from the mass ratio or from low-energy data, and eq. (11.9) gives the precise effect. Numerically this amounts to less than 1% corrections to the cross sections.

$$\frac{\delta g^2}{g^2} = \frac{\delta \alpha}{\alpha} - \frac{\delta s_\theta^2}{s_\theta^2} \ . \tag{9.5}$$

Taking into account these renormalization terms in $d\sigma^{ren}$, the final results turn out to be independent of the mass scale and all the ultraviolet pieces drop out. This is a very strong test on the consistency of the computation.

We thus two tests on the correctness of our computations, *viz*., the independence of the photon mass in the limit of zero photon mass, and the independence of the ultraviolet cut-off. Essentially these are checks on the various combinatorial factors. However, the calculation is quite involved, and due to the large cancellations inherent to gauge theories a small error can be of large consequence. For this reason we have also checked our expressions by applying Ward identities to the whole one-loop amplitude, even if the work involved was considerable. This is discussed in more detail in sect. 10.

## 10. Ward identities

In order to have a check on the finite part of the amplitude we computed the Ward identity (ref. [12]) of fig. 15. This Ward identity is computed for off-mass-shell vector bosons. The electron and positron are kept on-mass-shell. Moreover we used for convenience $q_1^2 = q_2^2$, where $q_1$ and $q_2$ are the vector boson momenta. Since the vector bosons are considered off-mass-shell the coupling of the Faddeev-Popov ghosts to the sources must be taken into account. The Feynman rules for these vertices are provided by the gauge transformations of the fields:

$$\begin{aligned}
&W_\mu^- \to W_\mu^- - ig(c_\theta W_\mu^0 + s_\theta A_\mu)\,\eta^- - igW_\mu^-(c_\theta \eta^3 + s_\theta \eta^0) - \partial_\mu \eta^+ \ , \\
&W_\mu^+ \to W_\mu^+ + ig(c_\theta W_\mu^0 + s_\theta A_\mu)\,\eta^+ - igW_\mu^+(c_\theta \eta^3 + s_\theta \eta^0) - \partial_\mu \eta^- \ , \\
&W_\mu^0 \to W_\mu^0 + igc_\theta(W_\mu^+ \eta^- - W_\mu^- \eta^+) - \partial_\mu \eta^3 \ , \\
&A_\mu \to A_\mu + igs_\theta(W_\mu^+ \eta^- - W_\mu^- \eta^+) - \partial_\mu \eta^0 \ .
\end{aligned} \tag{10.1}$$

In addition to the diagrams computed for the physical amplitude, self-energy, vertex and box one-loop diagrams with unphysical fields on the external lines must be

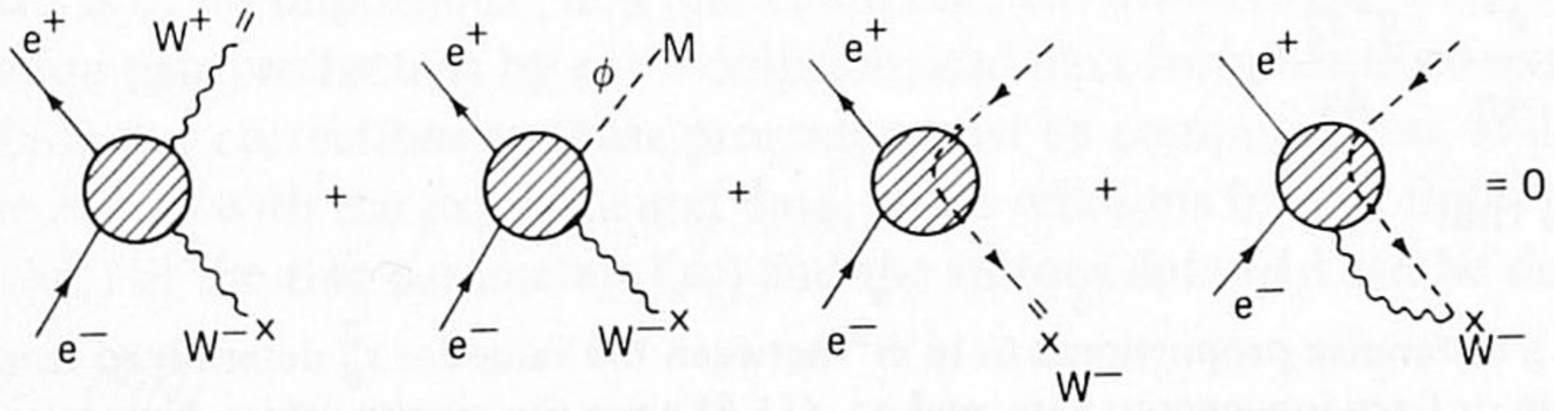


Fig. 15. Ward identity for the first-order amplitude.

calculated. All these terms are included in the blobs of fig. 15. The additional diagrams are computed analogously to the procedure given in the previous sections.

Fortunately the Ward identity of fig. 15 is not just one identity, but it contains subsets of diagrams, that satisfy Ward identities by themselves. Moreover the weak mixing angle and the Higgs mass can be varied. For instance $s_\theta = 0$ gives back the SU(2) model, containing less diagrams. We now describe globally the various steps in the calculation of fig. 15.

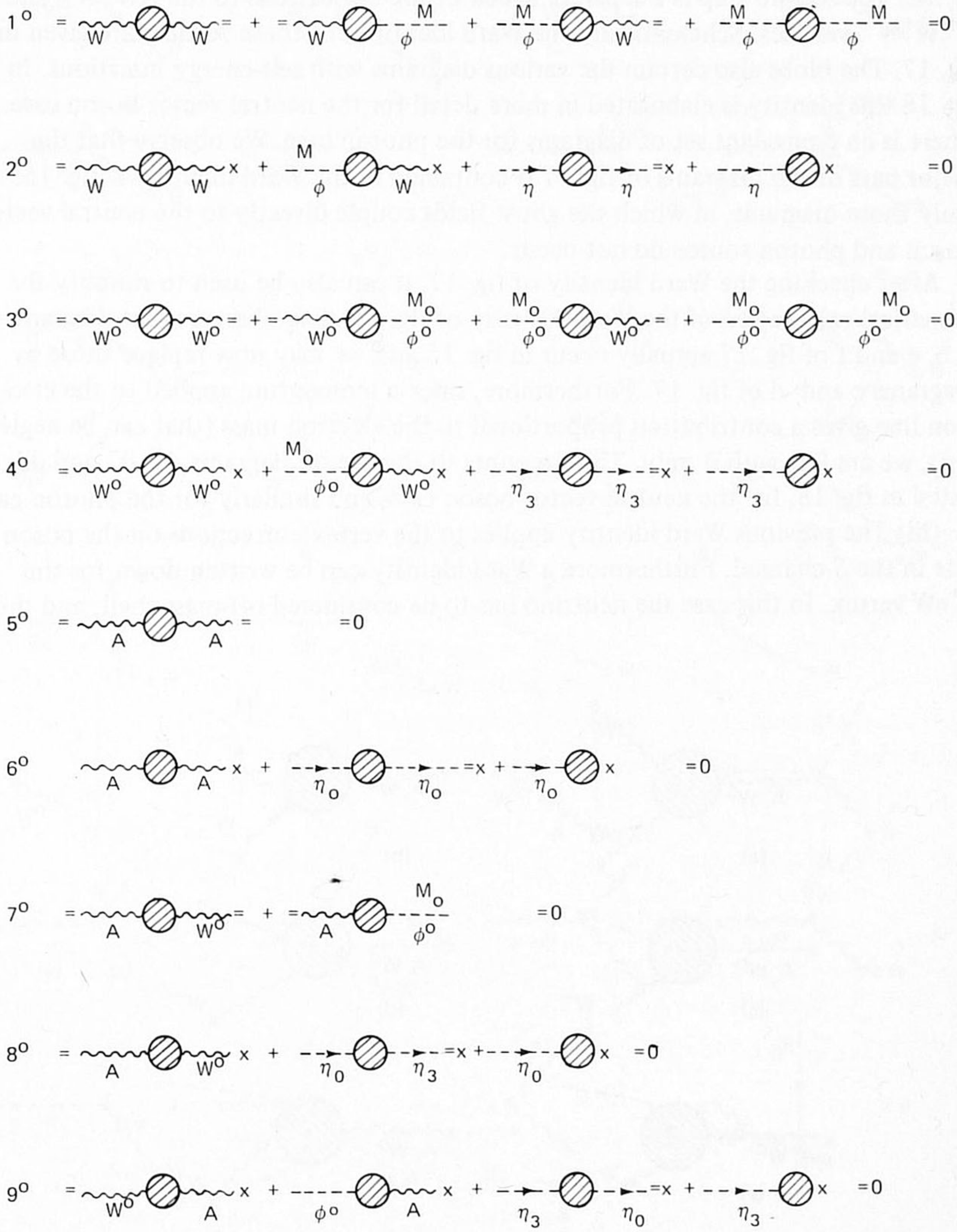


Fig. 16. Ward identities for self-energy diagrams.

(i) First we extended the set of self-energy diagrams with those of the ghost fields, and verified the Ward identities for self-energy insertions. These Ward identities are diagrammatically presented in fig. 16. $\eta^{\pm}$, $\eta^3$ and $\eta^0$ are the Faddeev-Popov ghost fields, corresponding to the vector fields and photon field. Blobs in fig. 16 present all the diagrams that contribute to the various self-energies and mixing of the fields. This completes a separate check on mixing and self-energy contributing terms in the Ward identity of fig. 15.

(ii) The second step is a separate check of the corrections to the $AW^+W^-$ and $W^0W^+W^-$ vertices. Schematically the Ward identities of these vertices are given in fig. 17. The blobs also certain the various diagrams with self-energy insertions. In fig. 18 this identity is elaborated in more detail for the neutral vector boson case. There is an equivalent set of diagrams for the photon case. We observe that the major part of the diagrams of fig. 17 is contained in the Ward identity of fig. 15. Only those diagrams, in which the ghost fields couple directly to the neutral vector boson and photon source do not occur.

After checking the Ward identity of fig. 17. it can also be used to simplify the numerical calculation of the Ward identity of fig. 15. One observes that diagrams a, b, e and f of fig. 17 actually occur in fig. 15 and we may now replace those by diagrams c and d of fig. 17. Furthermore, since a momentum applied to the electron line gives a contribution proportional to the electron mass (that can be neglected), we are left with d only. This amounts to the use of diagrams d1, d2 and d3, indicated in fig. 18, for the neutral vector boson case, and similarly for the photon case.

(iii) The previous Ward identity applies to the vertex corrections on the boson line in the $S$-channel. Furthermore a Ward identity can be written down for the $e^+\nu W$ vertex. In this case the neutrino has to be considered off-mass-shell, and there-

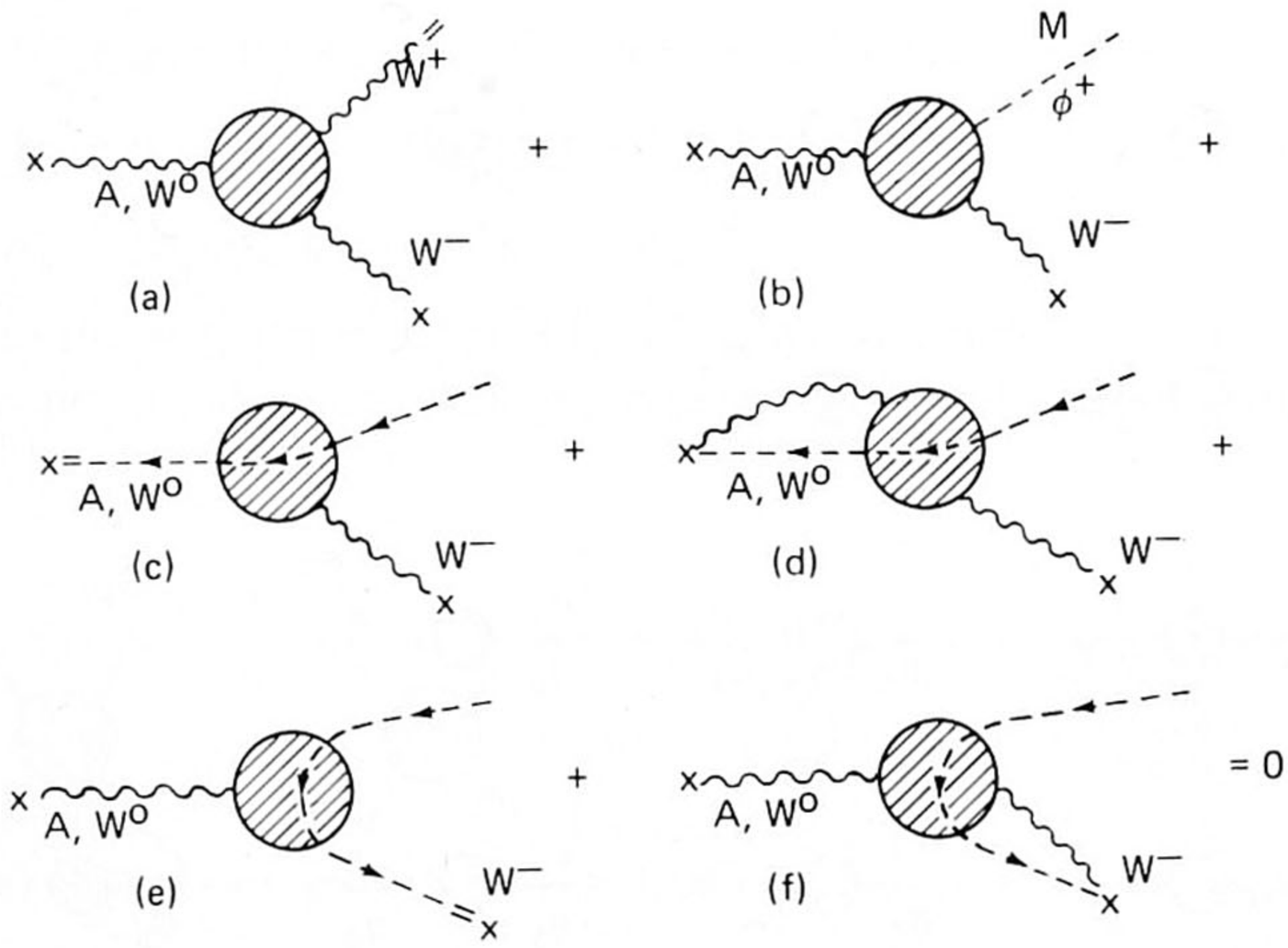


Fig. 17. Ward identity for one-loop $AW^+W^-$ and $W^0W^+W^-$ vertex corrections.

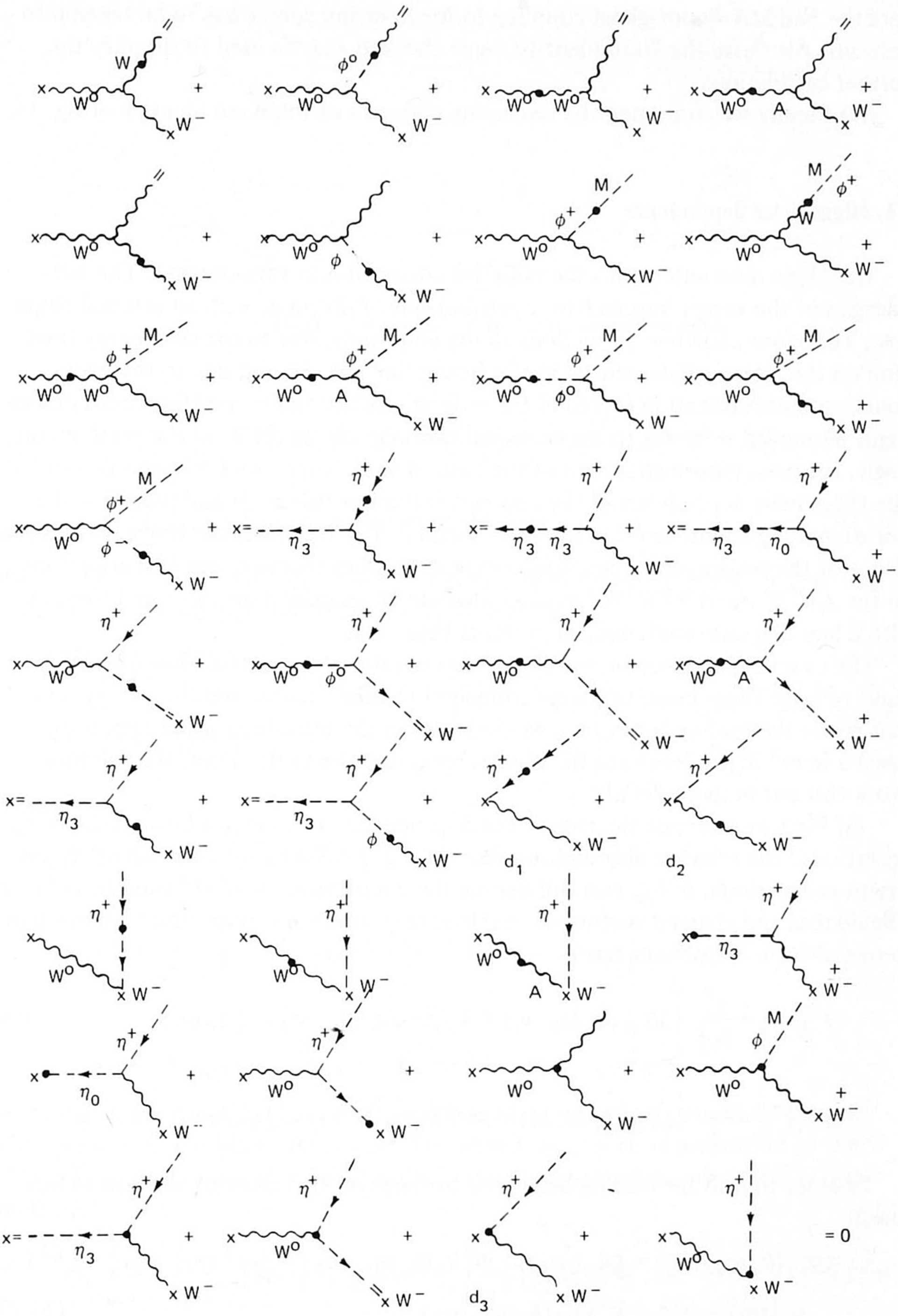


Fig. 18. Ward identity for one-loop $W^0W^+W^-$ vertex corrections.

fore the Faddeev-Popov ghost coupling to the neutrino source has to be taken into account. Also here the Ward identity, once checked, can be used to simplify the further calculations.

(iv) Finally we computed the remaining diagrams of the Ward identity of fig. 15.

## 11. Higgs-mass dependence

The Higgs mass enters into the radiative corrections in various ways. The self-energies of the vector bosons have contributions of diagrams with an internal Higgs line. Therefore, radiative corrections to the amplitude, due to the slef-energy insertion on the intermediate neutral vector boson line (fig. 5), and due to the wave-function renormalization (5.16) of the outgoing vector fields, are Higgs-mass dependent. Moreover, referring to the renormalization equation (9.4) of the weak mixing angle, the mass renormalizations of the neutral and charged vector boson determine the Higgs mass dependence of the renormalization of this angle and therefore the corresponding counterterm in the cross section. Also it defines the Higgs mass dependence of the renormalized coupling constant. Further there are several corrections to the $AW^+W^-$ and $W^0W^+W^-$ vertices that are Higgs mass dependent and there is also a box diagram, containing an internal Higgs line.

The exact dependence on the Higgs mass is quite complicated. However, in the limit of large Higgs mass, i.e., large compared to other masses and the energy, one can derive the leading behaviour. As explained in the introduction we expect at most a $\ln m^2$ dependence for the observable quantities in this limit. We will now work this out in more detail.

(i) First we examine the Higgs-mass dependence of the vector boson self-energy insertions. The relevant diagrams are those of fig. 19. We have to consider only the terms proportional to $\delta_{\mu\nu}$ and will denote the coefficients by $H^0(k^2)$ and $H^+(k^2)$ for the neutral and charged vector boson self-energy insertions, respectively. Written in terms of form factors one has:

$$H^0(k^2) = \frac{g^2}{3c_\theta^2}\,\{3B_{22}(k, M_0, m) + 3M_0^2 B_0(k, M_0, m) - \tfrac{3}{4}A_0(m)\}\,,$$

$$H^+(k^2) = \frac{g^2}{3}\,\{3B_{22}(k, M, m) + 3M^2 B_0(k, M, m) - \tfrac{3}{4}A_0(m)\}\,.$$

In order to find the leading behaviour for large $m$ the following relation can be used:

$$3B_{22}(k, m_1, m_2) = \tfrac{1}{2}A_0(m_2) - m_1^2 B_0(k, m_1, m_2) - \tfrac{1}{2}i\pi^3\,(m_1^2 + m_2^2 + \tfrac{1}{3}k^2)$$
$$- \tfrac{1}{2}(m_1^2 - m_2^2 - k^2)\,B_1(k, m_1, m_2)\,. \qquad (11.2)$$

We so obtain

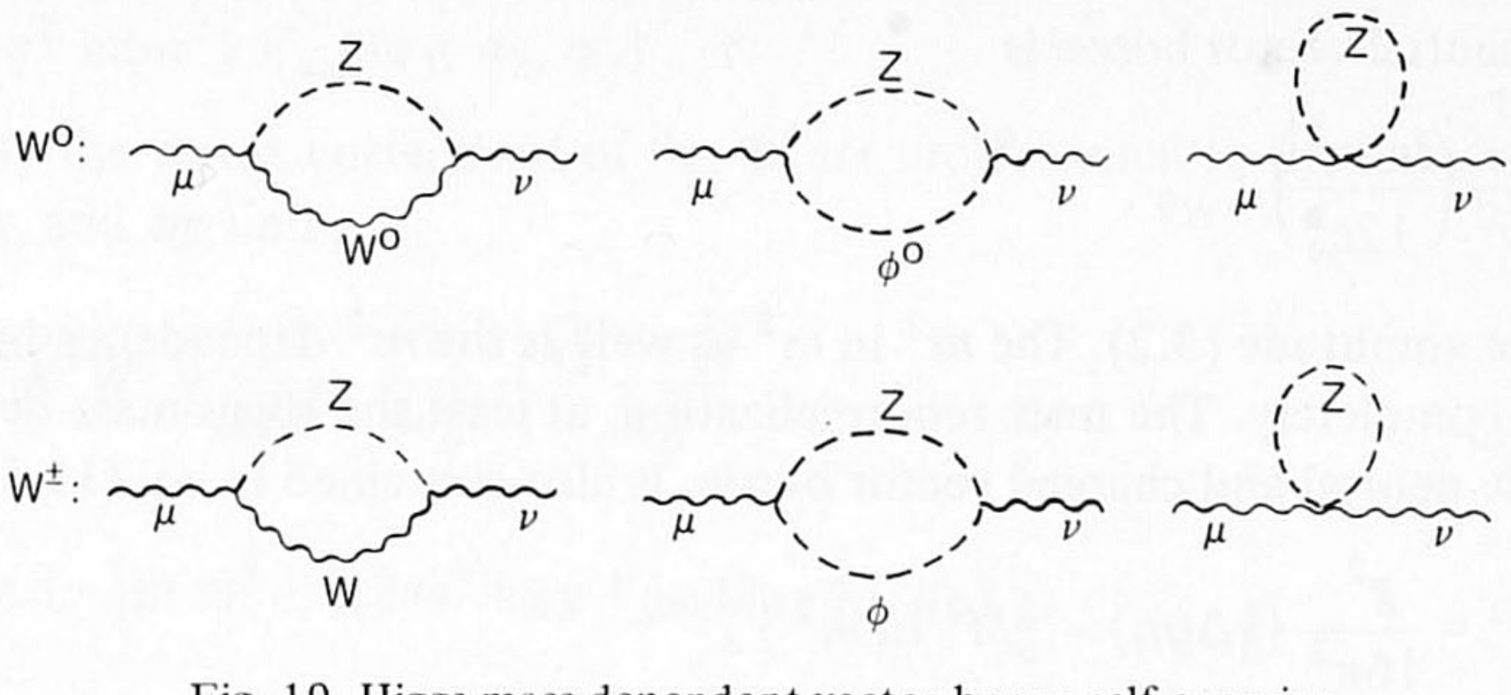


Fig. 19. Higgs-mass dependent vector boson self-energies.

$$H^0(k^2) = \frac{g^2}{3c_\theta^2}\ \{M_0^2(2B_0(k, M_0, m) - B_1(k, M_0, m)) + \tfrac{1}{2}(k^2 + M_0^2)\, B_1(k, M_0, m)$$

$$- \tfrac{1}{4}A_0(m) - \tfrac{1}{2}i\pi^2 m^2 + \tfrac{1}{2}m^2 B_1(k, M_0, m)\}\ , \qquad (11.3)$$

and similarly for $H^+$ with $M_0$ replaced by $M$, and without the factor $1/c_\theta^2$. In the limit $m \to \infty$ the asymptotic behaviour of $B_0$ and $B_1$ is

$$B_0 \underset{m\to\infty}{\sim} -i\pi^2 \ln m^2\ ,$$

$$B_1 \underset{m\to\infty}{\sim} \tfrac{1}{2}i\pi^2 \ln m^2\ . \qquad (11.4)$$

Thus

$$H^0(k^2) \underset{m\to\infty}{\sim} \frac{ig^2\pi^2}{3c_\theta^2}\ \{-\tfrac{5}{2}M_0^2 + \tfrac{1}{4}(k^2 + M_0^2) + \Delta(m)\} \ln m^2\ ,$$

$$H^+(k^2) \underset{m\to\infty}{\sim} \tfrac{1}{3}ig^2\pi^2\ \{-\tfrac{5}{2}M^2 + \tfrac{1}{4}(k^2 + M^2) + \Delta(m)\} \ln m^2\ , \qquad (11.5)$$

with

$$\Delta(m) = -\tfrac{1}{4}A_0(m) - \tfrac{1}{2}i\pi^2 m^2 + \tfrac{1}{4}i\pi^2 m^2 \ln m^2 = -\tfrac{1}{4}i\pi^2 m^2\ .$$

Note that these functions have $m^2 \ln m^2$ as leading term. Unfortunately this will not survive into the observable result. The wave-function renormalization of the charged vector boson is $(1 + \frac{1}{2}Z_W)$ and $Z_W$ can be extracted from eq. (11.5) (see sect. 5):

$$Z_W \underset{m\to\infty}{\to} \frac{1}{16\pi^4 i}[\tfrac{1}{3}i\pi^2 g^2]\ \tfrac{1}{4} \ln m^2 = \frac{g^2}{16\pi^2}\ [\tfrac{1}{12} \ln m^2]\ . \qquad (11.6)$$

After mass renormalization for the neutral vector boson the leading term in the radiative correction to the amplitude due to the self-energy insertion for the inter-

mediate neutral vector boson is

$$\frac{g^2}{16\pi^2}\left(\frac{\ln m^2}{12c_\theta^2}\right) L_{W0} \,. \tag{11.7}$$

$L_{W0}$ is the amplitude (3.2). The $m^2 \ln m^2$ as well as the $m^2$ dependence have disappeared completely. The mass renormalization, at least the Higgs-mass dependent part of the neutral and charged vector boson, is also contained in eq. (11.5):

$$\delta M^2 = \frac{g^2}{16\pi^2}\left\{\tfrac{1}{3}\Delta(m) - \tfrac{5}{6}M^2 \ln m^2\right\},$$

$$\delta M_0^2 = \frac{g^2}{16\pi^2 c_\theta^2}\left\{\tfrac{1}{3}\Delta(m) - \tfrac{5}{6}M_0^2 \ln m^2\right\}. \tag{11.8}$$

Using this we derive for the renormalization of the weak mixing angle

$$\delta s_\theta^2 = -\frac{\delta M^2 - c_\theta^2 \delta M_0^2}{M_0^2} = -\frac{g^2}{16\pi^2}\left[\tfrac{5}{6}s_\theta^2 \ln m^2\right]. \tag{11.9}$$

Again there is a screening effect.

(ii) Because the box diagram correction behaves as $1/m^2$ in the limit $m \to \infty$ we are left with corrections to the $AW^+W^-$ and $W^0W^+W^-$ vertices. The relevant diagrams are given by fig. 20. These vertex corrections are evaluated using the following generic expression for the loop integral (6.1):

$$\int dq \, \frac{(k_1+k_3)_\lambda (k_1+k_2)_\mu \, (k_2+k_3)_\nu}{(k_1^2+m_1^2)\,(k_2^2+k_2^2)\,(k_3^2+k_3^2)} \,, \tag{11.10}$$

with one of the internal masses $m_i$ equal to the Higgs mass. In leading order of large Higgs mass the loop integral (11.10) is

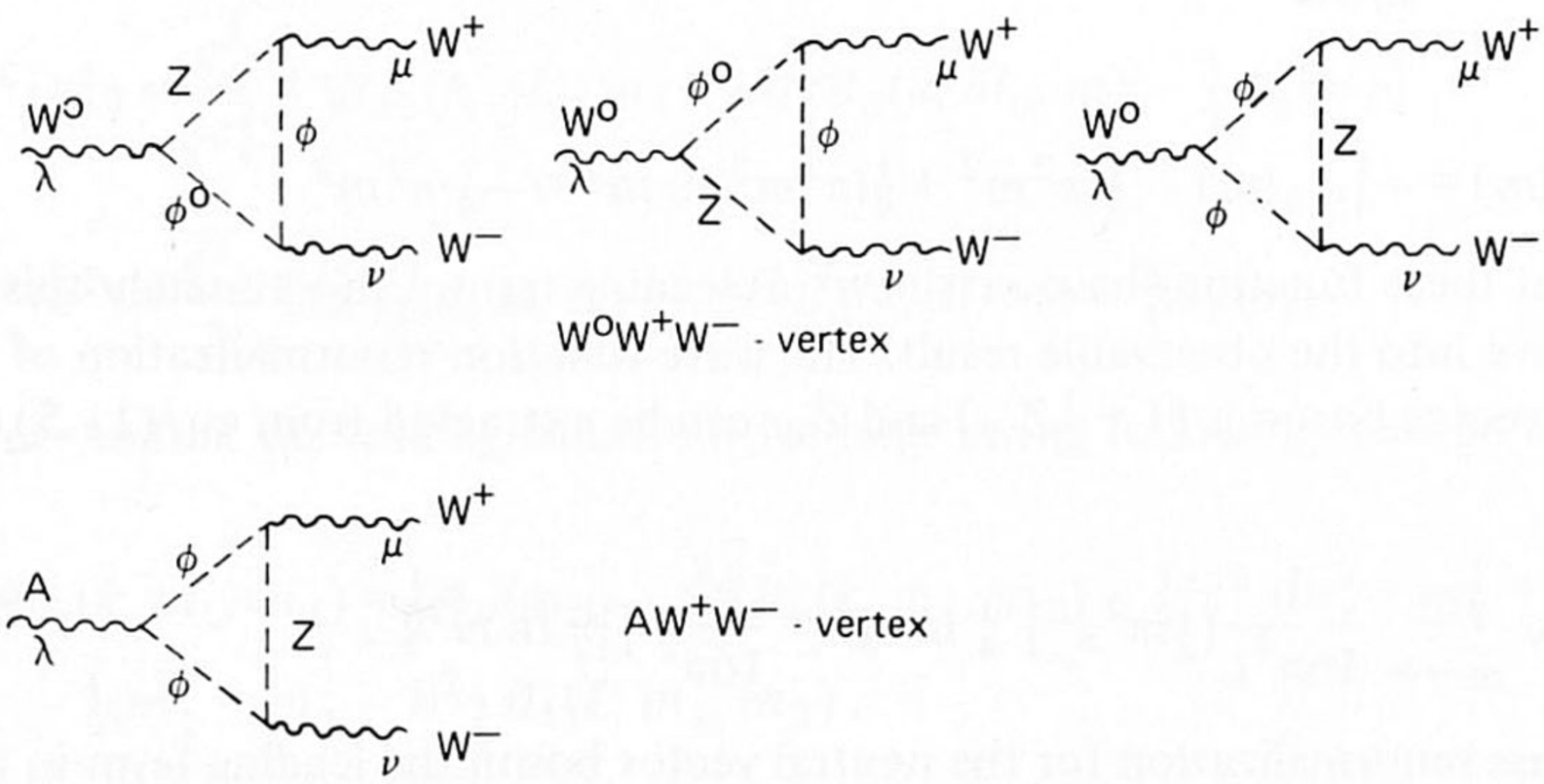


Fig. 20. Higgs-mass dependent $AW^+W^-$ and $W^0W^+W^-$ vertex corrections.

$$-\tfrac{1}{3}i\pi^2 \ln(m^2)\, V_{\mu\nu\lambda}(q_1, q_2, q_3)\,. \tag{11.11}$$

Apparently the vertex corrections of fig. 20 are proportional to the lowest-order 3W vertex, and we find

$$(\mathrm{W^0W^+W^-})\colon \frac{g^2}{16\pi^2}\ \frac{1}{4c_\theta^2} - \frac{(\frac{1}{2} - c_\theta^2)}{4c_\theta^2}$$

$$\times \{-\tfrac{1}{3}\ln m^2\}\ \{(2\pi)^4\, ic_\theta g\, V_{\mu\nu\lambda}(q_1, q_2, q_3)\}\,, \tag{11.12}$$

$$(\mathrm{AW^+W^-})\colon \frac{g^2}{16\pi^2}\ \{-\tfrac{1}{12}\ln m^2\}\ \{(2\pi)^4 is_\theta g V_{\mu\nu\lambda}(q_1, q_2, q_3)\}\,.$$

Taking into account the self-energy contributions of the intermediate vector boson and the wave-function renormalization of the charged vector bosons the following effective $\mathrm{W^0W^+W^-}$ interaction arises in the limit of large Higgs mass:

$$(\mathrm{W^0W^+W^-})_{\mathrm{eff}}\colon \quad \frac{g^2}{16\pi^2}\ \tfrac{1}{12}\ln m^2\ \frac{1}{2c_\theta^2}\ \{(2\pi)^4 i\, g c_\theta\, V_{\mu\nu\lambda}(q_1, q_2, q_3)\}\,. \tag{11.13}$$

For the effective $\mathrm{AW^+W^-}$ interaction there is no $\ln m^2$ dependence. Actually for $c_\theta = 1$ the result, eq. (11.13), coincides with the analysis of ref. [5].

(iii) Finally we must consider the Higgs-mass dependent radiative corrections due to the renormalization of the weak mixing angle and the coupling constant. The renormalization factor for the weak mixing angle manifests itself in two different ways: first by the counterterm

$$\delta s_\theta^2\ \frac{\partial}{\partial s_\theta^2}\,\sigma^0\,,$$

and second by the renormalization of the coupling constant, given in eq. (9.5). Because the renormalization of the fine structure constant $\alpha$ is Higgs-mass independent, the dependence of $\delta g^2$ on $m$ is given completely by $\delta s_\theta^2$:

$$\frac{\delta g^2}{g^2} = \frac{g^2}{16\pi^2}\ \{\tfrac{5}{6}\ln m^2\}\,.$$

That part of the amplitude, containing an intermediate photon (as in the lowest-order amplitude $L_\gamma$) contains no $\ln m^2$ dependence. The part of the amplitude, that contains an intermediate neutrino ($L_\nu$) depends on the Higgs mass due to the renormalization terms for the coupling constant $g$ and the wave-function renormalization of the charged vector bosons. The remaining Higgs-mass dependence in the limit of large Higgs mass is in the contributions of those corrections, that contain an intermediate neutral vector boson ($L_{\mathrm{W0}}$). The $\ln m^2$ terms enter through the vertex corrections (11.13), together with the renormalizations for weak mixing angle and the coupling constant $g$. Partial cancellations occur.

## 12. Results

Before presenting our results a few words are required in order to describe the reliability of the numerical answers. The reader has noticed that many diagrams have to be computed to obtain the physical amplitude. In these diagrams strings of $\gamma$-matrices have to be reduced or traces have to be evaluated, and typical gauge couplings involving the momenta of internal and external lines occur in the numerators of the loop integrals. This work was carried through with the help of SCHOONSCHIP (ref. [13]). The contraction of Lorentz indices needed special attention, since terms proportional to $(n-4)$ may give rise to finite contributions to the amplitude if poles in $(n-4)$ are present. A reduction to the form factors $A$, $B$, $C$ and $D$ of ref. [2] was made at the same time. Then these sometimes lengthy expressions were synthesized into a standard CDC-program, and evaluated using FORMF (ref. [14]), a numerical program for the form factors. Finally the renormalization part of the calculation was completed by linking the program to the program for the radiative corrections to $e^+e^- \to \mu^+\mu^-$ [2].

The results are presented in the plots (figs. 21–28). At various central mass energies ($E_{cm}$) the percentage corrections,

$$R(\varphi_{cm}, \omega) = \frac{d\sigma^1(\vartheta_{cm}, \omega)}{d\sigma^0(\vartheta_{cm})} ,$$

of the angular distributions are plotted for three values of the Higgs mass, *viz.*, 10, 100 and 1000 GeV. $d\sigma^1(\vartheta_{cm}, \omega)$ contains all one-loop corrections, bremsstrahlung and renormalization terms. $\omega$ denotes the upper limit of the bremsstrahlung energy. We have throughout used the values given by eq. (8.10).

We now discuss some features of the angular distribution for longitudinally polarized vector bosons.

The lowest-order cross section is of the order of $10^{-8}$ mb/sr (fig. 3), which is a small function of the cross section for the production of transversally polarized vector bosons (fig. 4). Just above threshold ($E_{cm} = 180$ GeV) the radiative corrections are a few percent. There is a peak around $\varphi_{cm} \approx 100°$, related to the minimum in the lowest-order cross section. In this region the corrections change sign. The Higgs-mass dependence is of the order of 2% for mass changes from 10 GeV to 100 GeV and from 100 GeV to 1000 GeV. Clearly the variation is proportional to $\ln m^2$. At higher total energy the Higgs-mass dependence increases slightly to about 5% in going from 10 to 1000 GeV.

Concerning the angular distribution for longitudinally and transversally polarized vector bosons we note the following. The lowest-order cross section (fig. 4) shows a strong peak in the forward direction due to the neutrino exchange in the $T$-channel (fig. 2). In this region of the scattering angle the cross section is of the order of $10^{-7}$ mb/sr. Just above threshold (fig. 24) the total radiative correction are a few percent. Higgs-mass dependence is also of the order of 4%, like in the longitudinal case, in going from 10 to 1000 GeV. At higher total energies (figs. 25–29) radiative correc-

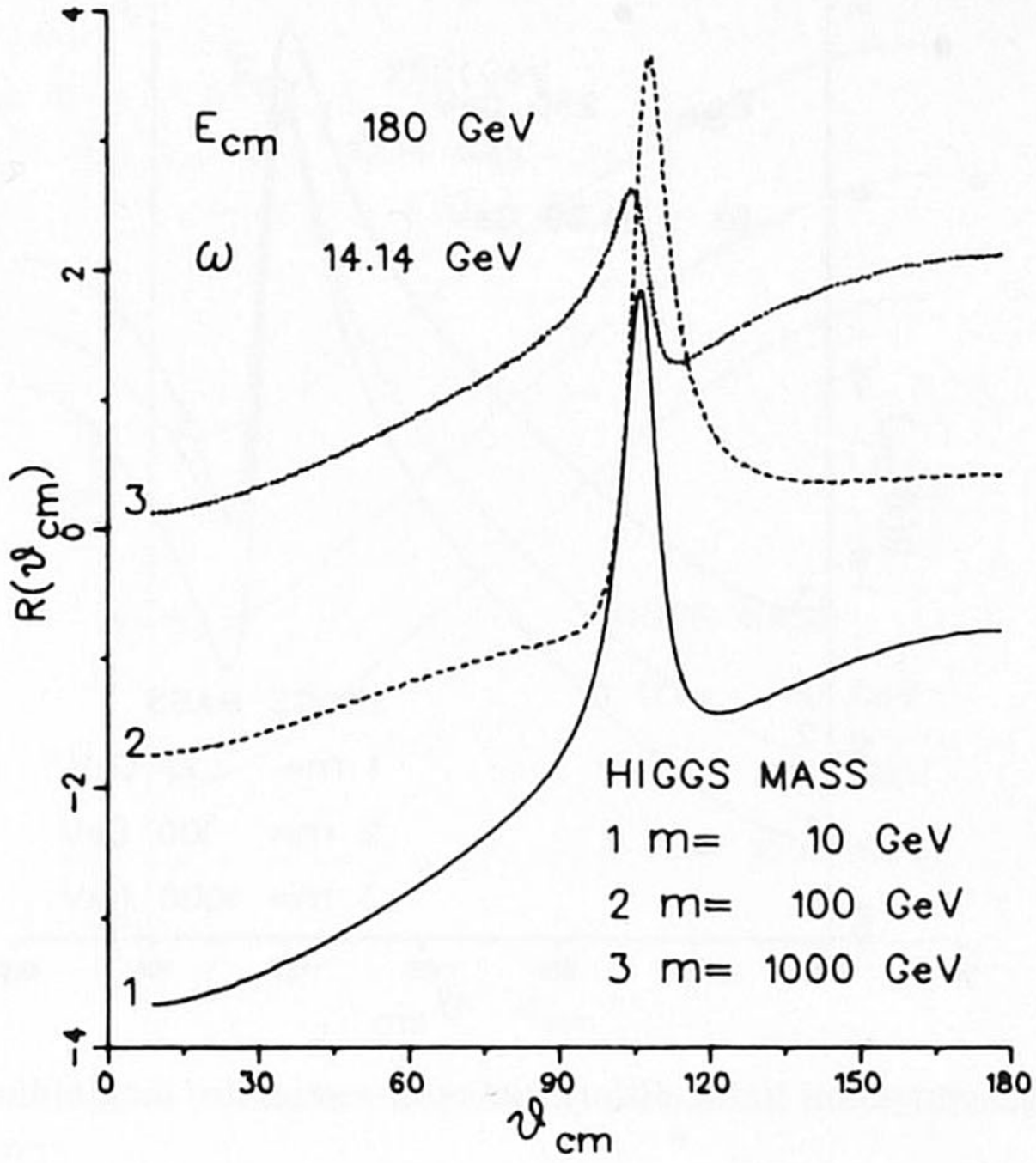


Fig. 21. Percentage correction to the differential cross section for longitudinally polarized vector bosons.

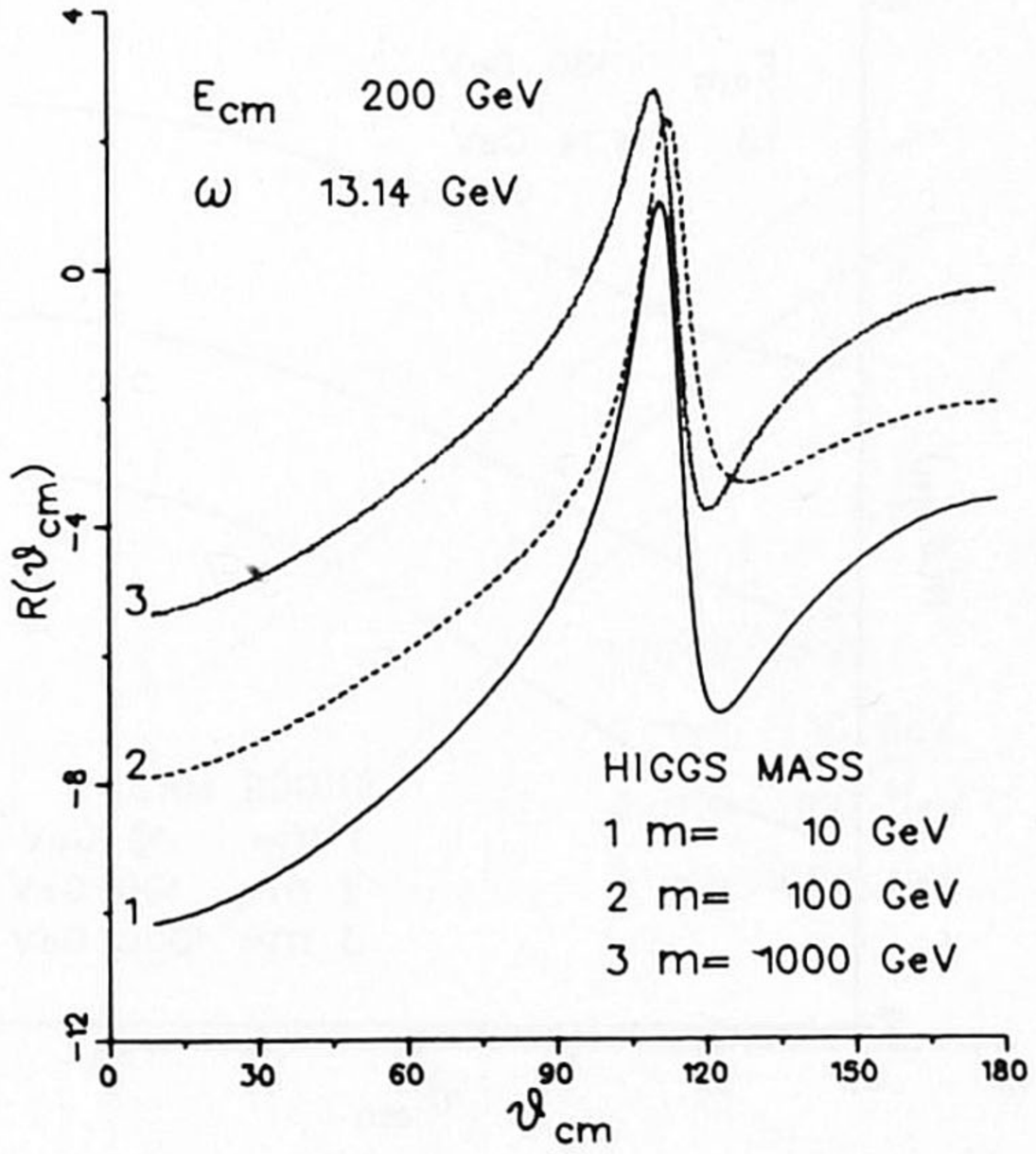


Fig. 22. Percentage correction to the differential cross section for longitudinally polarized vector bosons.

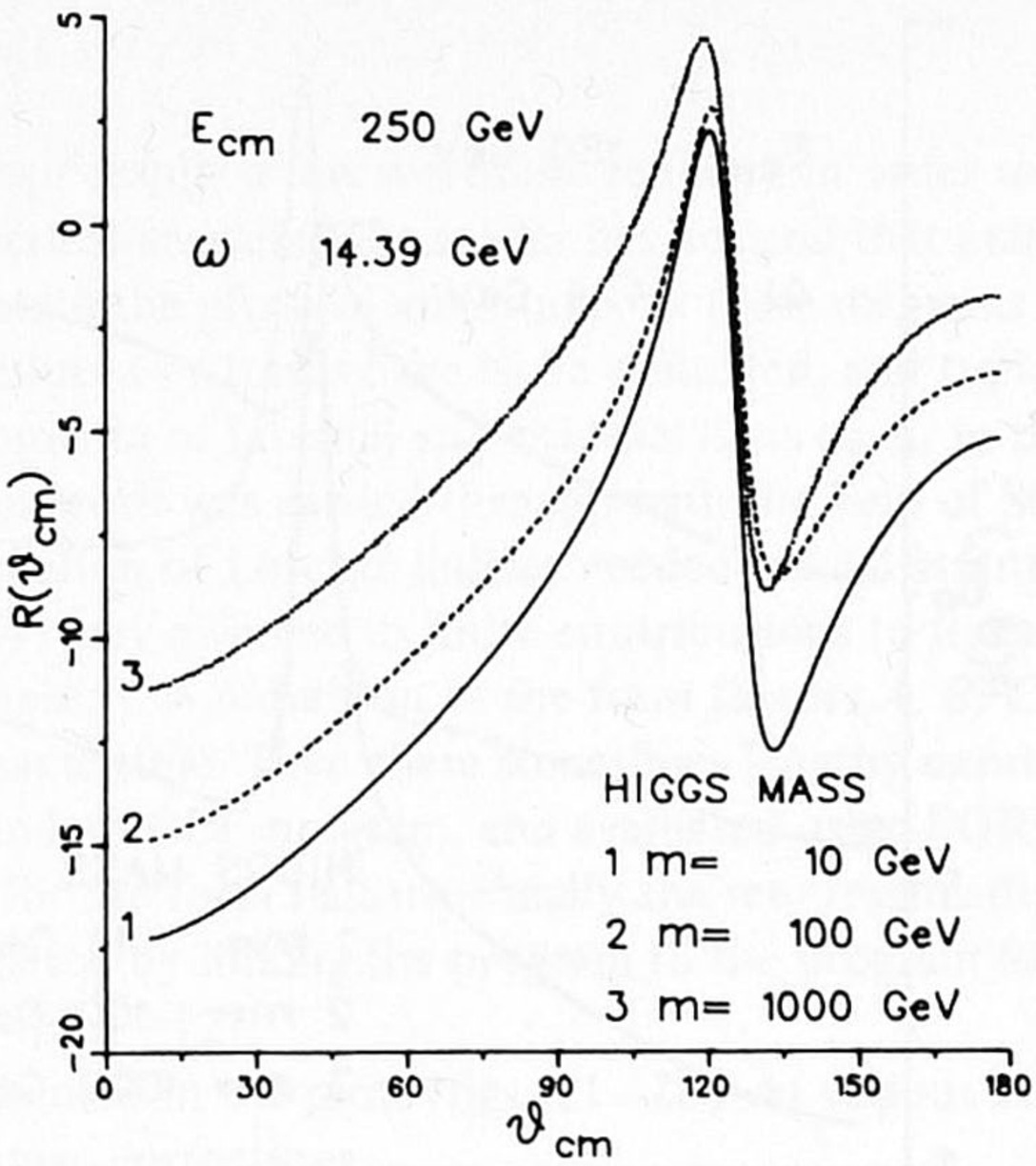


Fig. 23. Percentage correction to the differential cross section for longitudinally polarized vector bosons.

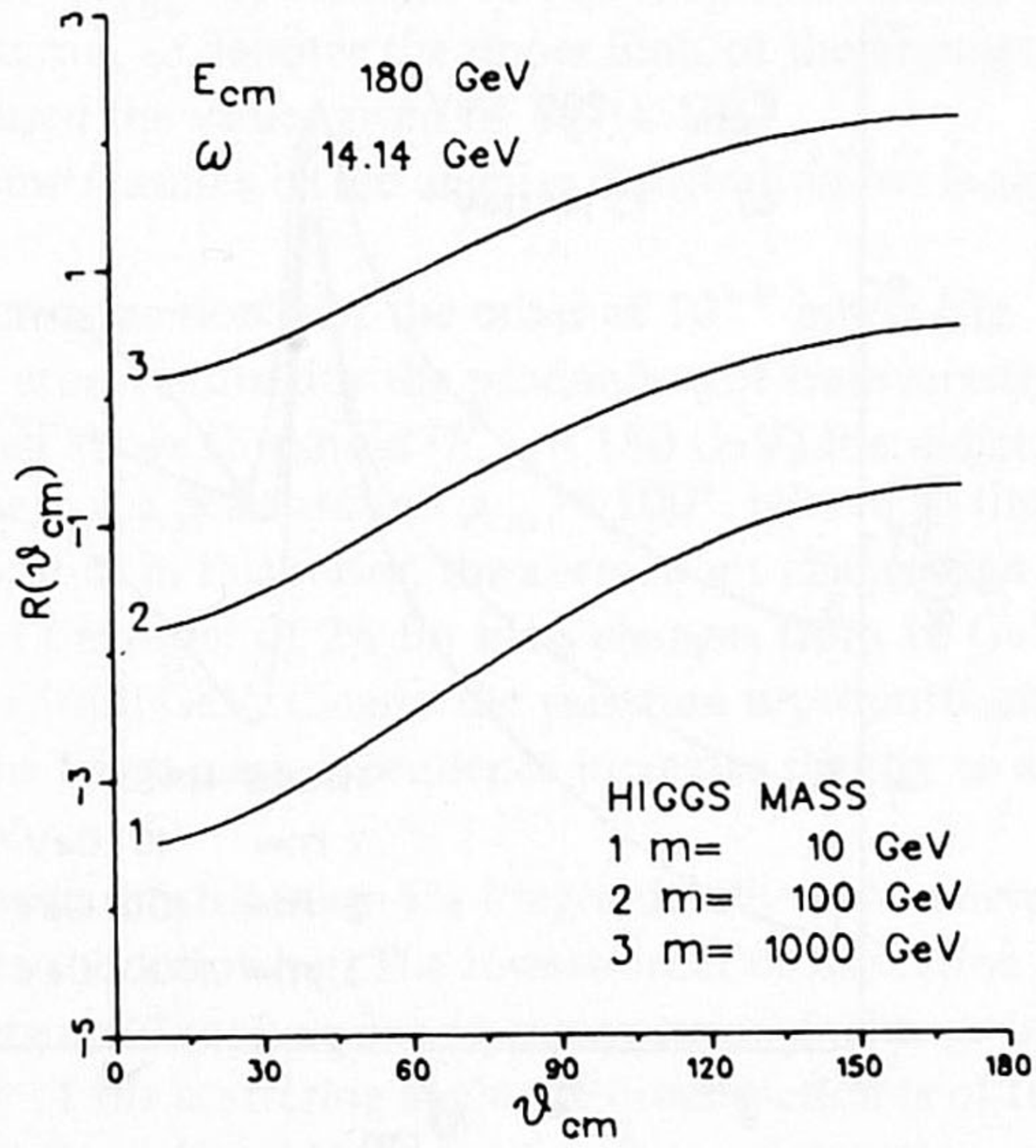


Fig. 24. Percentage correction to the differential cross section for longitudinally and transversally polarized vector bosons.

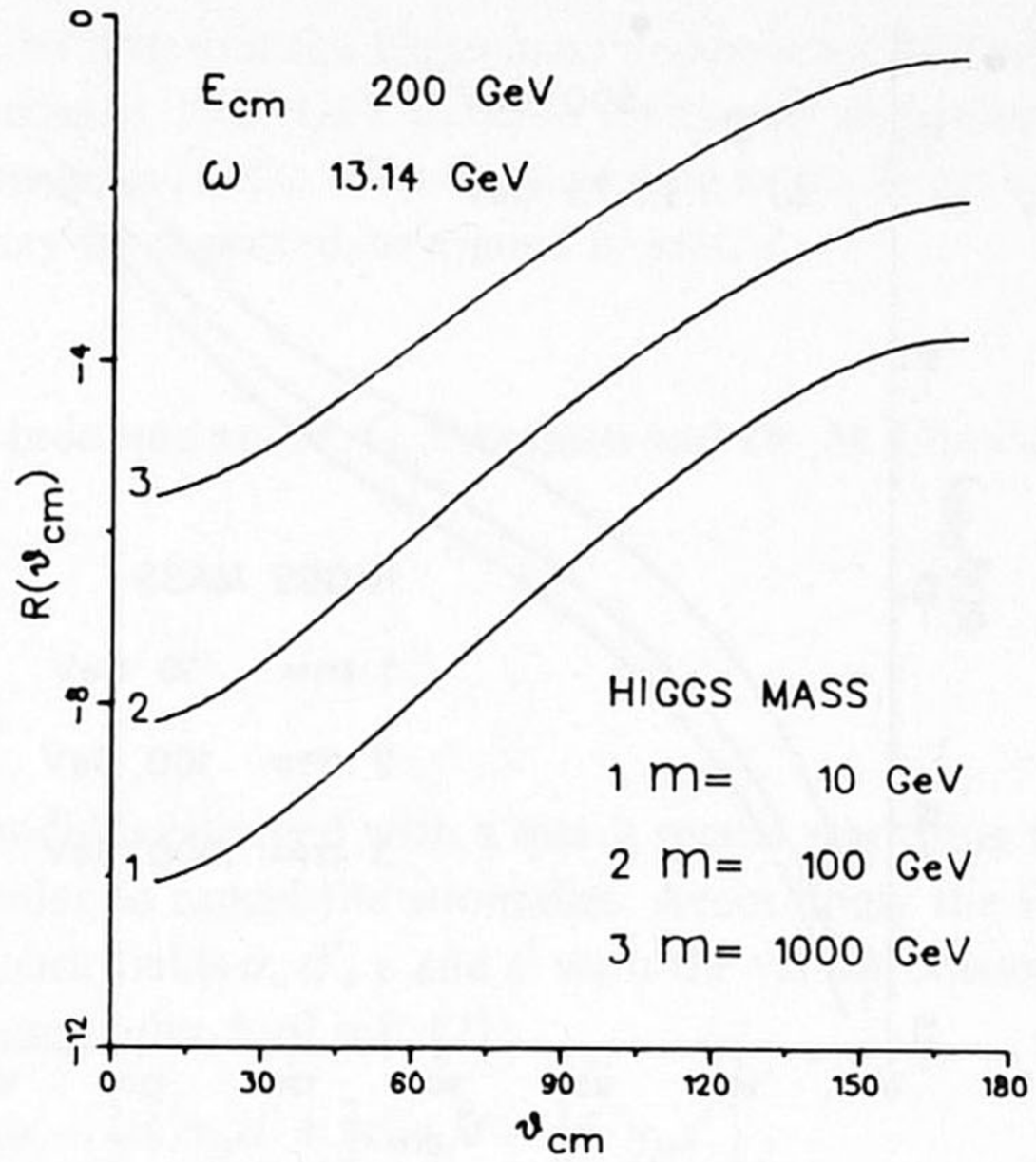


Fig. 25. Percentage correction to the differential cross section for longitudinally and transversally polarized vector bosons.

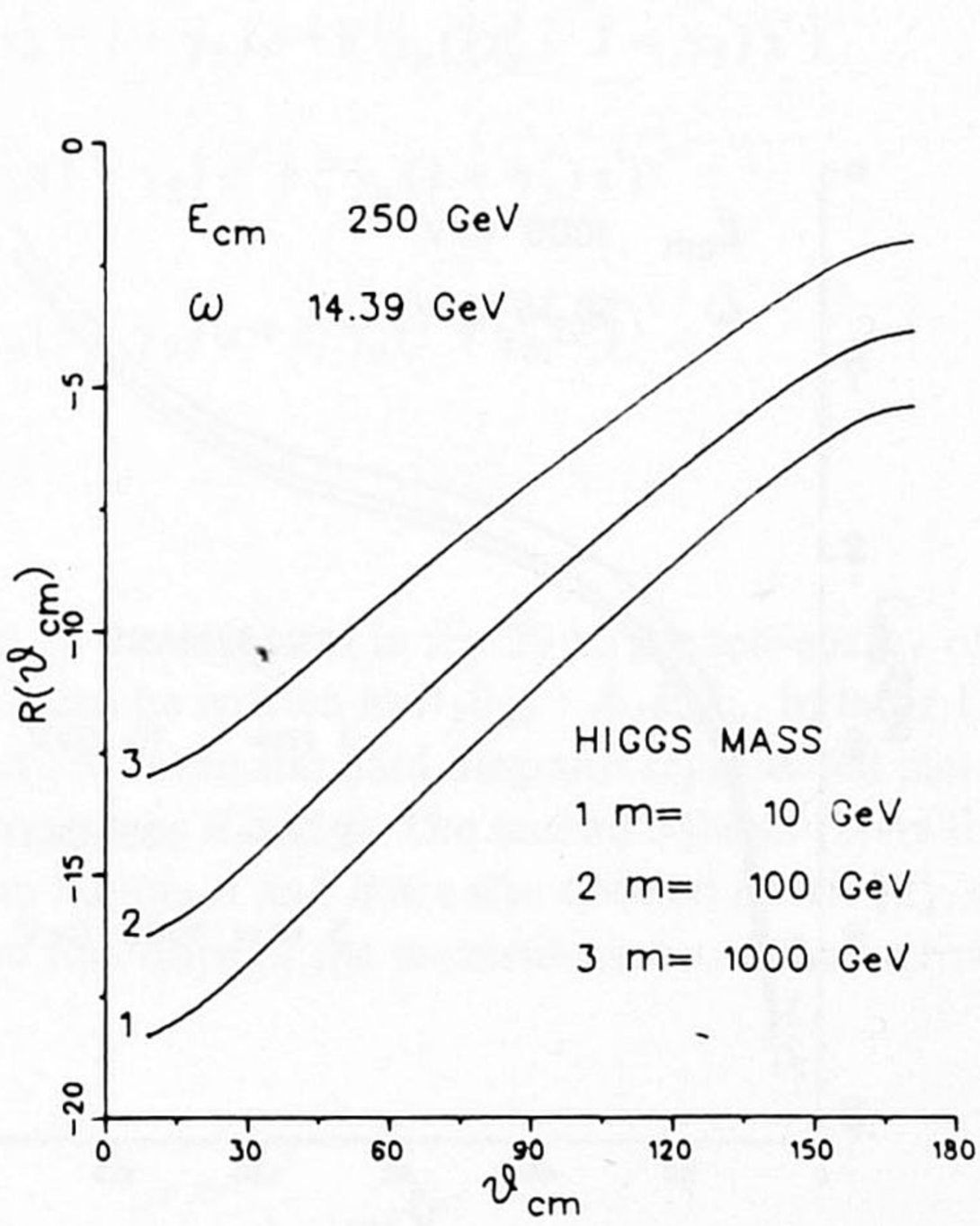


Fig. 26. Percentage correction the differential cross section for longitudinally and transversally polarized vector bosons.

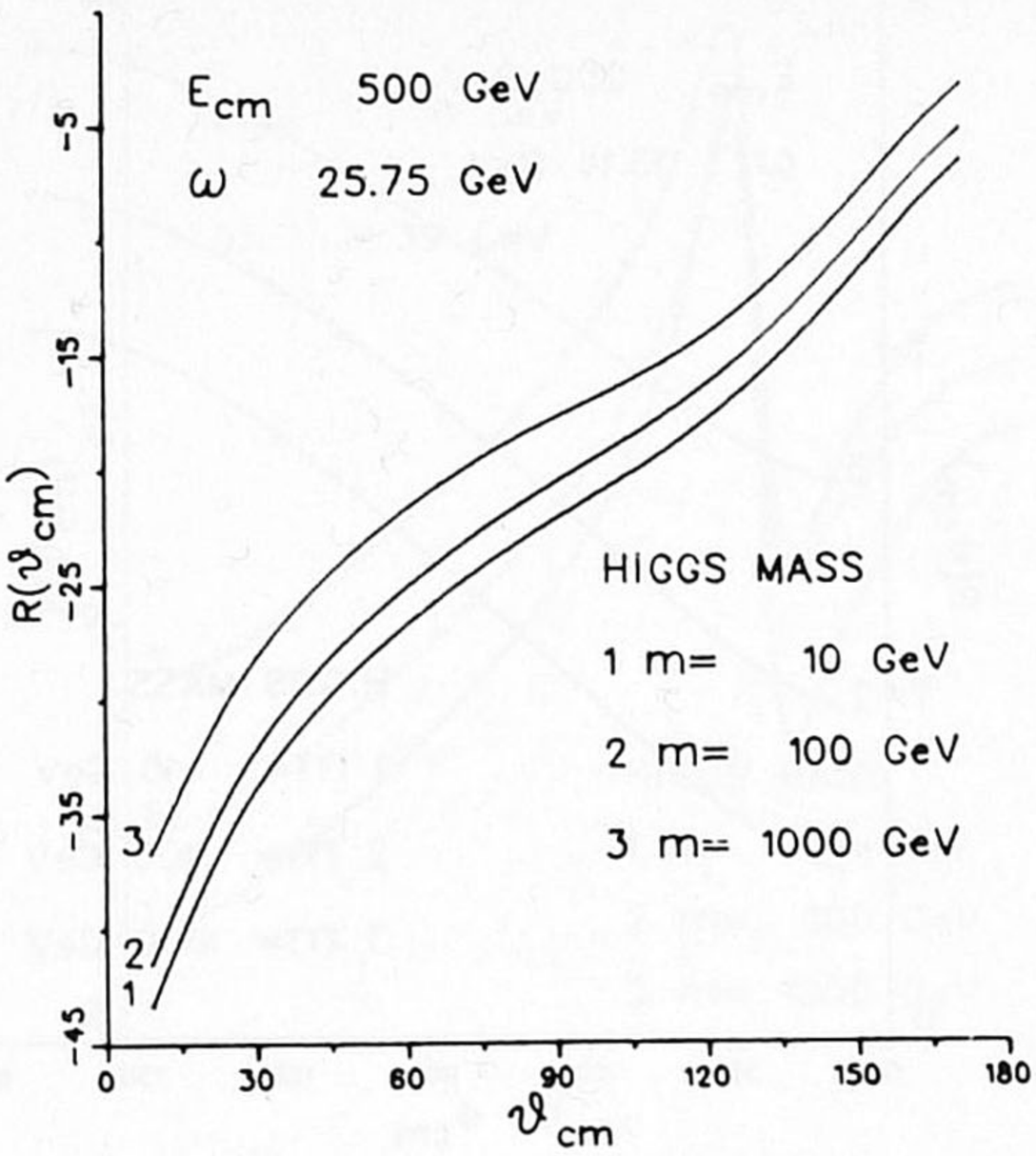


Fig. 27. Percentage correction to the differential cross section for longitudinally and transversally polarized vector bosons.

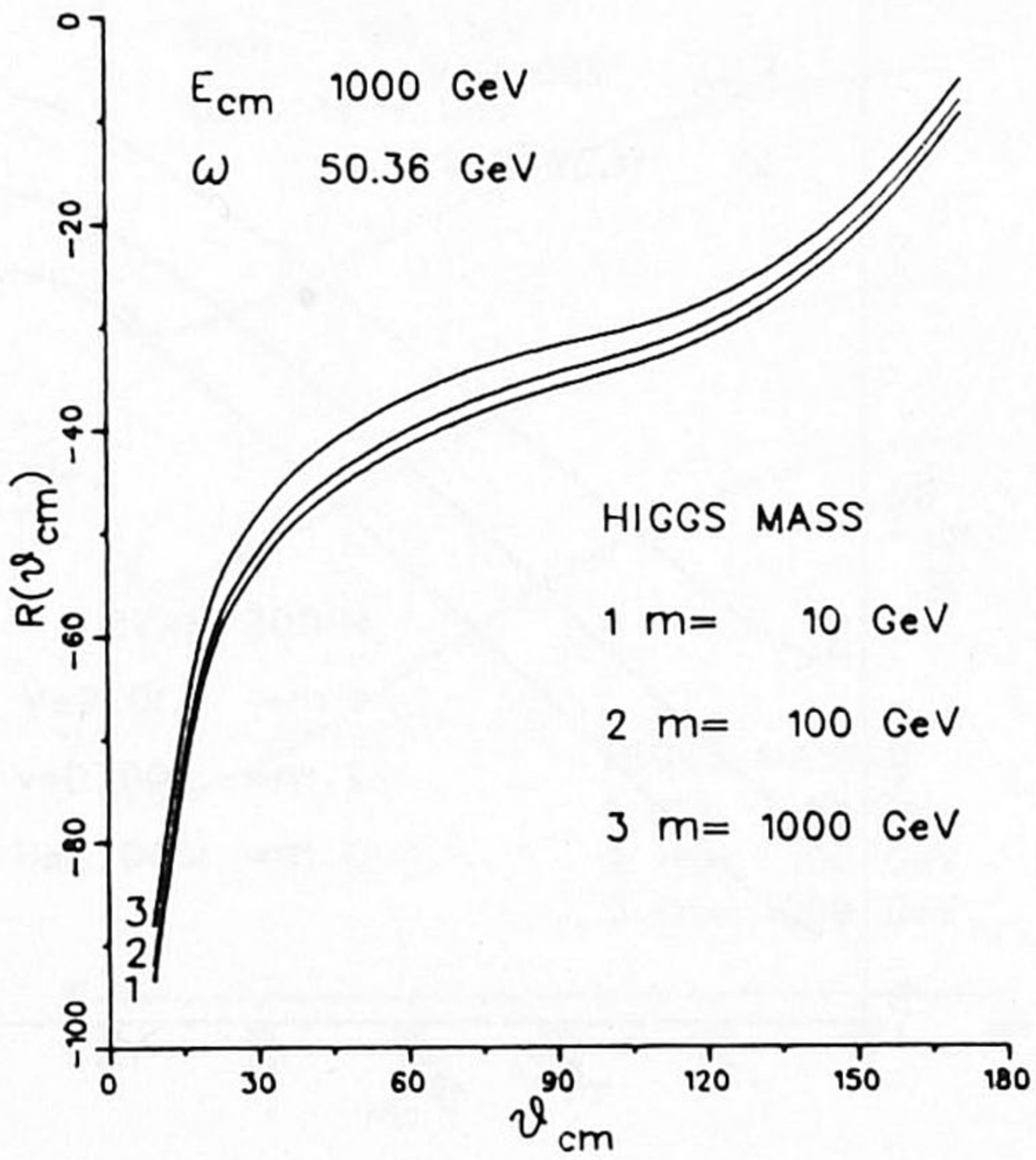


Fig. 28. Percentage correction to the differential cross section for longitudinally and transversally polarized vector bosons.

tions become considerable, and the Higgs mass dependence increases slightly. The plots with a Higgs mass of 1000 GeV must be seen as an indication. If the Higgs mass is of this order of magnitudes the effective coupling in the Higgs sector is quite strong and other effects may be expected, as argued in sect. 1.

The authors are indebted to Dr. G. Passarino and Dr. M. Consoli for many helpful discussions.

## Appendix A

The Weinberg model is enlarged with a quark sector according to the GIM-mechanism (ref. [4]) in order to cancel the anomalies. Accordingly the following interaction terms of the quark fields $u$, $d'$, $c$ and $s'$ with the vector bosons are added to the lagrangian given in appendix A of ref. [2]:

$$igs_\theta A_\mu \{\tfrac{2}{3}\bar{u}\gamma_\mu u - \tfrac{1}{3}\bar{d}'\gamma_\mu d' + \tfrac{2}{3}\bar{c}\,\gamma_\mu c - \tfrac{1}{3}\bar{s}'\gamma_\mu s'\}\,,$$

$$\frac{ig}{4c_\theta}\, W^0_\mu \{\bar{u}\,\gamma_\mu(-\tfrac{8}{3}\,s^2_\theta + 1 + \gamma_5)\,u + \bar{d}'\gamma_\mu(\tfrac{4}{3}s^2_\theta - 1 - \gamma_5)\,d'$$

$$+ \bar{c}\,\gamma_\mu(-\tfrac{8}{3}s^2_\theta + 1 + \gamma_5)\,c + \bar{s}'\gamma_\mu(\tfrac{4}{3}s^2_\theta - 1 - \gamma_5)\,s'\}\,,$$

$$\frac{ig}{2\sqrt{2}}\{W^+(\bar{u}\,\gamma_\mu(1+\gamma_5)\,d' + \bar{c}\,\gamma_\mu\,(1+\gamma_5)\,s')$$

$$+ W^-(\bar{d}'\gamma_\mu(1+\gamma_5)\,u + \bar{s}'\gamma_\mu(1+\gamma_5)\,c)\}\,.$$

## Appendix B

The contribution of the diagrams in fig. 29 to the self-energy of the vector bosons with 4-momentum $k$ can be written as $A_1\delta_{\mu\nu} + A_2 k_\mu k_\nu$. In table 1 we have expressed the factors $A_1$ and $A_2$ of seven standard diagrams represented pictorially in ref. [2], in terms of the form factors $A$ and $B$. The second column refers to these diagrams in ref. [2]. The form factors $A$ and $B$ are also defined in ref. [2], apart from a factor $i\pi^2$. These are functions of the momentum $k$ and the internal masses $m_1$ and

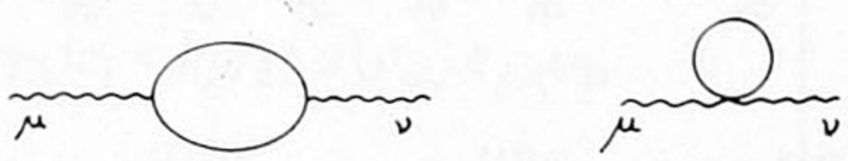


Fig. 29. Self-energy diagrams of the vector bosons.

Table 1
Expressions for the self-energy diagrams of the vector bosons

| $\Sigma^i_{\mu\nu}(k, m_1, m_2)$ | | $A_1$ | $A_2$ | $\frac{\partial}{\partial k^2} A_1$ |
|---|---|---|---|---|
| $i$ | | | | |
| 1 | S1 | $2i\pi^2(m_1^2 + m_2^2 + \frac{1}{3}k^2) + 10B_{22}$<br>$2k^2B_1 + (5k^2 - 2m_1^2)\,B_0 + 2A_0(m_2^2)$ | $-\frac{2}{3}i\pi^2 + 10B_{21} - 2B_0$<br>$+ 10B_1$ | $\frac{2}{3}i\pi^2 + 5(B_1 + B_{21}) + 2B_1 - 2k^2B_{1\mathrm{p}}$<br>$+ 5\,B_0 - B_{0\mathrm{p}}(5k^2 - 2m_1^2)$ |
| 2 | S9 | $8B_{22} - 4k^2B_1 - 4A_0(m_2^2)$ | $8B_{21} + 8B_1$ | $4B_{21} + 4k^2B_{1\mathrm{p}}$ |
| 3 | S6 | $4B_{22}$ | $4B_{21} + 4B_1 + B_0$ | $2B_{21} + 2B_1$ |
| 4 | S3 | $M^2B_0$ | | $-M^2B_{0\mathrm{p}}$ |
| 5 | S7 | $B_{22}$ | $B_{21} + B_1$ | $\frac{1}{2}(B_{21} + B_1)$ |
| 6 | S2 | $2m_1^2i\pi^2 + 3A_0(m_1^2)$ | | |
| 7 | S8 | $A_0(m_1^2)$ | | |

$m_2$. The last column of table 1 contains the derivative of $A_1$ with respect to $k^2$, to be used for wave-function renormalization of the charged vector boson fields. Note that $B_{0p}$ and $B_{1p}$ are defined as $-(\partial/\partial k^2)B_0$ and $-(\partial/\partial k^2)B_1$, respectively.

We will give the self-energy of the charged vector boson only. According to the notation of sect. 5 we have

$$\begin{aligned}
\Sigma^c_{\mu\nu}(k) = {} & c_\theta^2 \Sigma^1_{\mu\nu}(k, M_0, M) + \tfrac{1}{4}\Sigma^3_{\mu\nu}(k, M_0, M) + \frac{s_\theta^4}{c_\theta^4}\, \Sigma^4_{\mu\nu}(k, M_0, M) \\
& - 2c_\theta^2 \Sigma^5_{\mu\nu}(k, M_0, M) + \Sigma^4_{\mu\nu}(k, m, M) + \tfrac{1}{4}\Sigma^3_{\mu\nu}(k, m, M) \\
& + s_\theta^2 \Sigma^1_{\mu\nu}(k, \lambda, M) + s_\theta^2 \Sigma^4_{\mu\nu}(k, \lambda, M) - 2s_\theta^2 \Sigma^5_{\mu\nu}(k, \lambda, M) \\
& - \Sigma^6_{\mu\nu}(M) - \Sigma^7_{\mu\nu}(M) - c_\theta^2 \Sigma^6_{\mu\nu}(M_0) - \tfrac{1}{4}\Sigma^7_{\mu\nu}(M_0) - \tfrac{1}{4}\Sigma^7_{\mu\nu}(m) \\
& - \tfrac{1}{4}\Sigma^2_{\mu\nu}(k, 0, m_e) - \tfrac{1}{4}\Sigma^2_{\mu\nu}(k, 0, m_\mu) - \tfrac{3}{4}\Sigma^2_{\mu\nu}(k, m_p, m_n) \\
& - \tfrac{3}{4}\Sigma^2_{\mu\nu}(k, m_c, m_s)\,. \qquad \text{(B.1)}
\end{aligned}$$

Each term in eq. (B.1) corresponds to a different diagram contributing to the self-energy of the charged vector bosons.

The infrared-divergent part of the wave-function renormalization of the charged vector boson fields is given by the diagrams with an internal photon line. This divergence occurs in the derivative of the $B_0$ and $B_1$ form factors, computed at the pole $k^2 = -M^2$:

$$B_0(k, \lambda, M) = -i\pi^2 \int \mathrm{d}x \, \ln(-k^2x^2 + x(k^2 + \lambda^2) + (1 - x)\, m^2 - i\epsilon)\,,$$

$$B_1(k, \lambda, M) = i\pi^2 \int \mathrm{d}x \, x \, \ln(-k^2x^2 + x(k^2 + \lambda^2) + (1 - x)\, m^2 - i\epsilon)\,,$$

$$\frac{\partial}{\partial k^2} B_0(k, \lambda, M) \underset{\lambda \to 0}{=} \frac{i\pi^2}{M^2} \left(1 + \tfrac{1}{2} \ln \frac{\lambda^2}{M^2}\right) + \mathrm{O}(\lambda^2)\,,$$

$$\frac{\partial}{\partial k^2} B_1(k, \lambda, M) \underset{\lambda \to 0}{=} -\frac{i\pi^2}{M^2} \left(\tfrac{3}{2} + \tfrac{1}{2} \ln \frac{\lambda^2}{M^2}\right) + \mathrm{O}(\lambda^2)\,.$$

## Appendix C

The amplitude $\mathcal{A}_1$ for the process $\mathrm{e^+e^-} \to \mathrm{W^+W^-}$ (fig. 1) can be decomposed in several partially equivalent ways. For the vector boson vertex corrections we use the following decomposition:

$$\begin{aligned}
\mathcal{A}_1 = {} & \bar{u}(p_1)\, \gamma_\lambda (a_j + b_j\gamma_5)\, u(p_2)\, e_{1\mu} e_{2\nu} \\
& \times \{V_1^{\mathrm{b}} \delta_{\lambda\nu} q_{1\mu} + V_2^{\mathrm{b}} \delta_{\lambda\nu}\, q_{2\mu} + V_3^{\mathrm{b}} \delta_{\lambda\mu} q_{1\mu} + V_4^{\mathrm{b}}\, \delta_{\lambda\mu} q_{2\nu}
\end{aligned}$$

$$
\begin{aligned}
&+ V_5^{\mathrm{b}}\delta_{\mu\nu}q_{1\lambda} + V_6^{\mathrm{b}}\delta_{\mu\nu}q_{2\lambda} + V_7^{\mathrm{b}}q_{1\lambda}q_{1\mu}q_{1\nu}\\
&+ V_8^{\mathrm{b}}q_{1\lambda}q_{2\mu} + V_9^{\mathrm{b}}q_{1\lambda}q_{1\mu}q_{2\nu} + V_{10}^{\mathrm{b}}q_{1\nu}q_{1\mu}q_{2\lambda}\\
&+ V_{11}^{\mathrm{b}}q_{2\lambda}q_{2\nu}q_{1\mu} + V_{12}^{\mathrm{b}}q_{2\lambda}q_{2\mu}q_{1\nu} + V_{13}^{\mathrm{b}}q_{2\mu}q_{2\nu}q_{1\lambda}\\
&+ V_{14}^{\mathrm{b}}q_{2\lambda}q_{2\mu}q_{2\nu} + V_{15}^{\mathrm{b}}\epsilon_{\lambda\nu\mu\sigma}q_{1\sigma} + V_{16}^{\mathrm{b}}\epsilon_{\lambda\nu\mu\sigma}q_{2\sigma}\\
&+ V_{17}^{\mathrm{b}}\epsilon_{\lambda\nu\rho\sigma}q_{1\rho}q_{2\sigma}q_{1\mu} + V_{18}^{\mathrm{b}}\epsilon_{\lambda\nu\rho\sigma}q_{1\rho}q_{2\sigma}q_{2\mu}\\
&+ V_{19}^{\mathrm{b}}\epsilon_{\lambda\mu\rho\sigma}q_{1\rho}q_{2\sigma}q_{1\nu} + V_{20}^{\mathrm{b}}\epsilon_{\lambda\mu\rho\sigma}q_{1\rho}q_{2\sigma}q_{2\nu}\\
&+ V_{21}^{\mathrm{b}}\epsilon_{\nu\mu\rho\sigma}q_{1\rho}q_{2\sigma}q_{1\lambda} + V_{22}^{\mathrm{b}}\epsilon_{\nu\mu\rho\sigma}q_{1\rho}q_{2\sigma}q_{2\lambda}\}\,.
\end{aligned}
$$

In the case of correction to the $e^+\nu W$ vertex

$$
\begin{aligned}
\mathcal{A}_1 &= \bar{u}(p_1)\,\gamma_\lambda(\not{p}_2 + \not{q}_2)\,\gamma_\nu(a_j + b_j\gamma_5)\,u(p_2)\\
&\times(V_{11}^{\mathrm{f}}\delta_{\lambda\mu} + V_{12}^{\mathrm{f}}q_{1\lambda}q_{1\mu} + V_{13}^{\mathrm{f}}q_{1\lambda}p_{1\mu})\,e_{1\mu}e_{2\nu}\,.
\end{aligned}
$$

For the $e^-\nu W$ vertex

$$
\begin{aligned}
\mathcal{A}_1 &= \bar{u}(p_1)\,\gamma_\mu(\not{p}_2 + \not{q}_2)\,\gamma_\lambda(a_j + b_j\gamma_5)\,u(p_1)\\
&\times(V_{21}^{\mathrm{f}}\delta_{\lambda\nu} + V_{22}^{\mathrm{f}}q_{2\lambda}q_{2\nu} + V_{23}^{\mathrm{f}}q_{2\lambda}p_{2\nu})\,e_{1\mu}e_{2\nu}\,,
\end{aligned}
$$

and for the box diagrams finally,

$$
\begin{aligned}
\mathcal{A}_1 &= \bar{u}(p_1)\,\gamma_\lambda(a_j + b_j\gamma_5)\,u(p_2)\,e_{1\mu}e_{2\nu}\\
&\times\{\delta_{\lambda\nu}(B_1^x q_{1\mu} + B_3^x p_{1\mu} + B_4^x p_{2\mu})\\
&+ \delta_{\lambda\nu}(B_5^x q_{1\nu} + B_7^x p_{1\nu} + B_8^x p_{2\mu})\\
&+ B_{10}^x q_{1\lambda}q_{1\mu}q_{1\nu} + B_{11}^x q_{1\lambda}q_{1\nu}p_{1\mu}\\
&+ B_{12}^x q_{1\lambda}q_{1\nu}p_{2\mu} + B_{13}^x q_{1\lambda}q_{1\mu}p_{1\nu}\\
&+ B_{14}^x q_{1\lambda}q_{1\mu}p_{2\nu} + B_{15}^x q_{1\lambda}p_{1\mu}p_{1\nu}\\
&+ B_{16}^x q_{1\lambda}p_{2\mu} + B_{17}^x q_{1\lambda}p_{2\nu}p_{1\mu}\\
&+ B_{18}^x q_{1\lambda}p_{2\nu}p_{2\mu} + B_{19}^x q_{1\lambda}\delta_{\mu\nu}\}\\
&+ B_{20}^x\bar{u}(p_1)\,\gamma_\lambda(a_j + b_j\gamma_5)\,u(p_2)\,\epsilon_{\lambda\mu\nu\sigma}q_{1\sigma}e_{1\mu}e_{2\nu}\\
&+ B_{21}^x\bar{u}(p_1)\,(\gamma_\mu(\not{p}_2 + \not{q}_2)\,\gamma_\nu(a_j + b_j\gamma_5))\,u(p_2)\,e_{1\mu}e_{2\nu}\,.
\end{aligned}
$$

Note that the last term can be rewritten in terms of the previous terms with the help of the identity

$$
\gamma_\mu\gamma_\nu\gamma_\lambda = \gamma_\mu\delta_{\nu\lambda} - \gamma_\nu\delta_{\mu\lambda} + \gamma_\lambda\delta_{\mu\nu} + \epsilon_{\mu\nu\lambda\sigma}\gamma_5\gamma_\sigma\,.
$$

However, we have kept this term for computational convenience.

## References


[1] G. 't Hooft and M. Veltman, Nucl. Phys. B153 (1979) 365; Utrecht preprint (Nov., 1978).
[2] G. Passarino and M. Veltman, Nucl. Phys. B160 (1979) 151.
[3] M. Consoli, Nucl. Phys. B160 (1979) 208.
[4] S. Bludman, Nuovo Cim. 9 (1958) 433;
S. Glashow, Nucl. Phys. 22 (1961) 579;
S. Glashow, J. Iliopoulos and L. Maiani, Phys. Rev. D2 (1970) 1285;
S. Weinberg, Phys. Rev. Lett. 19 (1967) 1264.
[5] M. Veltman, Acta Phys. Pol. B8 (1977) 475;
M. Veltman, Phys. Lett. 70B (1977) 253.
[6] D. Dicus and V. Mathur, Phys. Rev. D7 (1973) 3111;
B.W. Lee, C. Quigg and H. Tracker, Phys. Rev. Lett. 38 (1977) 888; Phys. Rev. D16 (1977) 1519;
J.S. Kang, Maryland preprint 77-254.
[7] M. Chanowitz, M. Furman and I. Hinchliffe, Nucl. Phys. B159 (1979) 225.
[8] W. Alles, Ch. Boyer and A.J. Buras, Nucl. Phys. B119 (1977) 125;
K. Gaemers and K. Gunaros, Z. Phys. C 1 (1979) 259.
[9] F. Berends, K. Gaemers and R. Gastmans, Nucl. Phys. B57 (1973) 381.
[10] F. Berends, K. Gaemers and R. Gastmans, Nucl. Phys. B63 (1973) 381.
[11] F. Berends, K. Gaemers and R. Gastmans, Nucl. Phys. B68 (1974) 541.
[12] G. 't Hooft and M. Veltman, Diagrammar, CERN report (1973).
[13] M. Veltman SCHOONSCHIP, a CDC program for symbolic evaluation of algebraic expressions, CERN preprint (1967);
H. Strubbe, Comp. Phys. Comp. 8 (1974) 1.
[14] M. Veltman, FORMF, a CDC program for numerical evaluation of form factors, Utrecht (1979).